Monthly Notices
of the
ROYAL ASTRONOMICAL SOCIETY

MNRAS **509,** 345–366 (2022)
Advance Access publication 2021 October 21

https://doi.org/10.1093/mnras/stab3026

The role of impacts on the atmospheres on the moons of outer giants

Catriona A. Sinclair★ and Mark C. Wyatt

Institute of Astronomy, Madingley Road, Cambridge CB3 OHA, UK

Accepted 2021 October 15. Received 2021 September 3; in original form 2021 May 11

ABSTRACT

We investigate the comparative effect of impacts by trans-Neptunian Objects on the atmospheres of the moons Ganymede, Callisto, Europa, and Titan. We derive an analytic prescription for the 'stalling mass' (i.e. the atmosphere mass at which equilibrium between erosion and volatile delivery occurs), which is tested against a numerical model, demonstrating that the behaviour of the atmosphere matches the analytic prediction, albeit with stochastic events causing orders of magnitude variability. We find that bombardment, neglecting other effects, predicts atmosphere erosion on Ganymede, Callisto, and Europa leading to masses in quantitative agreement with the observed atmospheres. The predicted masses are relatively insensitive to the impactor size and velocity distributions, but sensitive to impactor density and volatile content. Crucially, we find that in this model the frequent arrival of 1–20 km-sized objects sets the quiescent atmosphere masses of the different moons, with atmospheres returning to these levels on ∼100 Myr time-scales at current bombardment levels, and larger impactors causing stochastic excursions to larger atmosphere masses. This quiescent level is higher on Titan than the Jovian moons due to the typically slower impact velocities, but to recreate Titan's massive current atmosphere an additional volatiles contribution is needed, which may be provided by impact-triggered outgassing. If so, the predicted mass is then dependent on the outgassing efficiency and the volatile mass contained in the crust, both of which are uncertain. This work highlights the role that impacts may have played in shaping the atmosphere evolution of outer Solar system moons, and the importance of stochastic effects.

Key words: planets and satellites: atmospheres – planets and satellites: formation – planetary systems.

1 INTRODUCTION

The moons of the giant planets in our Solar system display a large degree of variation among their properties. The three largest Jovian moons – Ganymede, Callisto and Europa – are diverse in terms of their mass and inferred internal structures, but are similar in terms of the low atmospheric pressures estimated on their surfaces. Saturn's moon Titan is similar in size to Ganymede and Callisto, but is unique for being the only moon in the Solar system to possess a substantial atmosphere. This atmosphere is composed mainly of N_2 with a smaller CH_4 component and has a surface pressure of 1.5 bar (Strobel 1982; Coustenis 2005).

These differences are informative, as they are signatures of the different formation and evolutionary processes acting on the moons. These processes are numerous, but of particular interest is the effect of impacts by small objects on the atmosphere because such impacts are an inevitable consequence of Solar system formation models and are clearly evidenced by the extensive cratering seen on the surfaces of the outer moons (see for example Strom & Croft 1993; Korycansky & Zahnle 2005; Mah & Brasser 2019; Bell 2020). Impacts result in the delivery of mass and energy to any potential atmosphere, and thus can both erode existing atmospheres and deliver volatiles that replenish the atmosphere. Furthermore, impacts are capable of melting the surface of a target body, releasing previously trapped volatiles in a process known as impact-triggered outgassing (Artemieva & Lunine 2005; Kraus, Senft & Stewart 2011).

In the 'snowplough' impact prescription from Melosh & Vickery (1989) the inertia of the atmosphere determines whether an atmosphere is lost or gained. Within this framework impactors above critical mass and velocity values are assumed to remove the entire atmosphere mass above the tangent plane at the impact site, while impactors below these values are assumed to contribute their entire volatile content to the atmosphere. As a result of this approach, once an atmosphere begins to erode the critical impactor mass decreases, meaning that a greater number of impacts are erosive (and simultaneously fewer are capable of delivering volatiles) and therefore the atmosphere continues to erode until it is stripped to a bare rock. Conversely, an atmosphere that begins to grow is destined to continue to accrete volatiles, resulting in runaway growth. Alternatively, in the 'cookie cutter' model of Walker (1986) it is the specific energy delivered to the atmosphere that determines the evolution. Within this model it is possible for a stable equilibrium atmosphere mass at which impact erosion and volatile delivery are balanced can exist.

Neither of these approaches is entirely correct, with more recent hydrodynamic simulation results typically falling between the two extremes (see for example: Svetsov 2007; Shuvalov 2009; Shuvalov et al. 2014; Schlichting, Sari & Yalinewich 2015; Denman et al. 2020; Kegerreis et al. 2020, among others). These are capable of predicting the atmosphere mass-loss and impactor mass retained as a function of the size, density, and composition of the target and impactor, as well as the atmosphere properties and impact velocity.

★ E-mail: cas213@cam.ac.uk

The Shuvalov (2009) impact prescription adopted in the remainder of this paper is similar in this respect to the Walker (1986) model, and therefore results in the predicted existence of stable equilibria as described in Wyatt, Kral & Sinclair (2020). This phenomenon is discussed in relation to this study in Section 2.4.

Comparative studies of impact-induced atmospheres on the outer satellites were conducted by both Zahnle et al. (1992) and Griffith & Zahnle (1995) using this 'snowplough' impact prescription. The results of these two studies are similar, finding that impacts result in overall growth of an atmosphere on Titan and erosion on Ganymede and Callisto as a result of the typically slower impact velocities predicted for Titan in comparison to the Jovian moons. Significant stochastic variation was observed in Griffith & Zahnle (1995) due to the inclusion of a Monte Carlo impactor sampling approach.

The prescription from Shuvalov (2009) was used in Marounina et al. (2015) to investigate the evolution of Titan's atmosphere during a proposed late heavy bombardment scenario. The results from this study suggest that impacts cause erosion of an initially massive atmosphere on Titan, but growth of a thin atmosphere from an initially bare state. This contrasts to the results from Zahnle et al. (1992) arises primarily from the use of the atmosphere mass-loss prescription from Shuvalov (2009). This prompted Marounina et al. (2015) to include impact-triggered outgassing, using the prescriptions from Kraus et al. (2011) and Sekine et al. (2011), which predicted the release of a significant mass of volatiles into the atmosphere, resulting in atmospheric growth. This proposed origin of Titan's atmosphere is supported by the measured D-H ratio and excess CH_4 in comparison to CO, which suggest that cometary volatiles are not the likely direct source of the atmospheric material on Titan (Coustenis 2005). Rather, the presence of CH_4 (which should rapidly undergo photolysis) and normal C isotopic ratios in Titan's massive atmosphere suggest a continuing source of methane (Owen 2004), possibly resulting from episodic outgassing from clathrate hydrates stored in a solid shell above an ammonia-enriched water ocean (Tobie, Lunine & Sotin 2006; Stofan et al. 2007).

The conclusions regarding atmospheric evolution of the moons of the giant planets are not only dependent on the impact prescription, but also on the assumed impactor properties. These complexities have not been considered systematically in previous comparative studies of multiple outer moons, yet they provide additional evidence that can be used to constrain the properties of the impactor population. Furthermore, the importance of the stochastic delivery of large impactors first described in Griffith & Zahnle (1995) is particularly important when considering small satellites with low impact rates. Another crucial unknown that has not been explored systematically in the literature is the initial atmosphere mass, which can determine whether the same population of impactors will result in atmosphere growth or erosion on a given target.

In this work, we aim to investigate the comparative effect of impacts on four of the five largest moons in the outer Solar system, excluding Io due to the substantial volcanic outgassing and the significant influence of Jupiter's magnetic field which make impacts a less significant driver of atmospheric evolution, to attempt to understand the diversity of atmospheres observed among these moons. To do this we make use of the prescriptions from Shuvalov (2009) to parametrize the outcome of impacts with a range of properties. While these prescriptions have some uncertainties, e.g. in the regimes where the results are extrapolated to impacts with parameters not covered in the simulations, we will take them at face value to explore their implications. These prescriptions are applied within an extension of the analytic prediction for the behaviour of the atmosphere due to a population of impactors from Wyatt et al. (2020), allowing us to investigate the quantitative behaviour of the atmosphere, the stable atmosphere 'stalling' mass (at which the rate of atmosphere erosion is balanced by the rate of volatile delivery) towards which it evolves and the time-scale of this evolution. The sensitivity of these predictions to some of the many free parameters that determine the outcome of an impact on the atmosphere can then be investigated. We also make use of the numerical model for stochastic atmosphere evolution due to impacts presented in Sinclair et al. (2020), which allows us to investigate the importance of the inherently stochastic nature of impacts.

In Section 2, the prescriptions used to parametrize the effect of an impact on the atmosphere are described, the analytic prediction for the behaviour of the atmosphere and the stalling mass is presented, and the numerical model for stochastic atmosphere evolution is also described. The properties assumed for the outer moons and the nominal impacting population of comets are described in Sections 3 and 4, respectively. The analytic results, without including the prescription for impact-triggered outgassing, are presented in Section 5 for the nominal impactor properties. In Section 6, the corresponding numerical results are discussed and compared to the analytic predictions. The sensitivity of these predictions to the properties of the impacting comets (density, volatile content, size distribution, and dynamics) is investigated in Section 7. Finally, in Section 8 the contribution of impact-triggered outgassing to the analytic results is investigated using a simple toy model. Our results are discussed in Section 9 and our conclusions presented in Section 10.

2 ATMOSPHERE EVOLUTION DUE TO IMPACTS

The behaviour of an atmosphere undergoing impacts will be determined by the ratio of atmosphere mass gain resulting from the impacts (m^+) to atmosphere mass-loss (m^-),

$$f_v = \frac{m^+}{m^-}. \quad (1)$$

The atmosphere mass gain can result from volatiles in the mass accreted after an impact, or from volatiles trapped in the planet that are released by impact-triggered outgassing. The atmosphere mass-loss can be a direct result of the crater formation at the impact site, or through non-local atmosphere mass-loss caused by shock waves propagating through the planet. How we calculate the various contributions to atmosphere mass evolution is discussed in the following sections. In Section 2.1, the local contributions from cratering and the global contributions of giant impacts to m^+ and m^- are described, with the treatment of airless bodies and the lower atmosphere limit described in Section 2.2. The prescription used to include the atmosphere mass contribution from impact-triggered outgassing is described in Section 2.3. In Section 2.4, the analytic approximation used to calculate the characteristic stalling atmosphere mass (nominally without including the effect of impact-triggered outgassing) and the overall behaviour of the atmosphere for a given body and population of impactors from f_v is explained. Finally in Section 2.5 the numerical code used to stochastically model the evolution of an atmosphere is described.

2.1 Parametrization of cratering impacts

The atmospheric outcome of an impact depends on the energy of the impactor and the properties of the target body surface and atmosphere. In this work, we follow the approach described in

Kral et al. (2018), Wyatt et al. (2020), and Sinclair et al. (2020), which use the impact prescriptions from Shuvalov (2009) combined with analytic expressions for the polar cap mass-loss limit from Schlichting et al. (2015). The inclusion of non-local giant impact-induced atmosphere mass-loss is discussed below. This allows the calculations of the mass of atmosphere removed (m_a^-) and the mass of volatiles delivered (m_a^+) relative to the impactor mass ($m_{\rm imp} = \frac{\pi}{6}\rho_{\rm imp} D^3$).

The Shuvalov (2009) cratering prescriptions are parametrized in terms of the dimensionless erosional efficiency (η), which is itself a function of the impactor properties (size D, density $\rho_{\rm imp}$, and velocity $v_{\rm imp}$) and target properties (escape velocity $v_{\rm esc}$, density $\rho_{\rm tar}$, atmosphere scale height H, and atmospheric density at the base of the atmosphere ρ_0) through

$$\eta = \left(\frac{D}{H}\right)^3 \left[\left(\frac{v_{\rm imp}}{v_{\rm esc}}\right)^2 - 1\right] \left[\frac{\rho_{\rm imp}\rho_{\rm tar}}{\rho_0(\rho_{\rm imp} + \rho_{\rm tar})}\right]. \quad (2)$$

The scale height depends on the atmosphere temperature T, mean molecular weight μ, and target body gravity g through $H = \frac{k_{\rm B}T}{\mu m_{\rm H} g}$. Assuming an isothermal ideal atmosphere, and provided that $\delta \equiv m_{\rm atm}/M_{\rm tar} \ll 1$ the atmosphere density is related to the mass of the atmosphere through

$$m_{\rm atm} = \delta M_{\rm tar} = 4\pi R_{\rm tar}^2 H \rho_0. \quad (3)$$

The prescription from Shuvalov (2009) for cratering impacts gives the fractional atmosphere mass lost due to a single impact by a body with mass $m_{\rm imp}$ to be

$$\frac{m_{\rm atmloss}}{m_{\rm imp}} = \left[\left(\frac{v_{\rm imp}}{v_{\rm esc}}\right)^2 - 1\right] \chi_{\rm a}(\eta), \quad (4)$$

where

$$\begin{aligned}\log\left(\chi_{\rm a}(\eta)\right) = &-6.375 + 5.239\left(\log(\eta)\right) - 2.121\left(\log(\eta)\right)^2 \\ &+ 0.397\left(\log(\eta)\right)^3 - 0.037\left(\log(\eta)\right)^4 \\ &+ 0.0013\left(\log(\eta)\right)^5. \end{aligned} \quad (5)$$

As in Sinclair et al. (2020), we modify equation (5) for values of $\eta > 10^6$ to ensure that absolute atmosphere mass-loss increases with increasing impactor mass in the high η regime. This modification takes the form of a power law, fit to $\chi_a(10^4 \leq \eta \leq 10^6)$, applied to $\eta > 10^6$ with a correction to avoid a discontinuity in χ_a at $\eta = 10^6$

$$\log\left(\chi_a(\eta > 10^6)\right) = -0.6438\eta + 0.4746. \quad (6)$$

The polar cap limit is included, in line with the theoretical framework presented in Schlichting et al. (2015). This limit arises from the constraint that the maximum atmosphere mass that can be ejected by a single cratering impact cannot be greater than the mass of the atmosphere contained in the polar cap, the volume of the atmosphere that lies above the plane tangent to the surface of the target at the impact site (Schlichting et al. 2015). This is included into the impact prescription as an upper bound on the value of $m_{\rm atmloss}$ calculated for a single impactor,

$$m_{\rm max} = m_{\rm cap} = 2\pi\rho_0 H^2 R_{\rm tar}. \quad (7)$$

This cap mass is the same as the atmosphere mass assumed to be ejected by any eroding impactor in the framework of Zahnle et al. (1992) and Melosh & Vickery (1989). However in our prescription only the largest impactors are capable of ejecting this mass of atmosphere, and most impactors instead result in the loss of a smaller fraction of the atmosphere mass.

The effects of 'giant' impacts are included through the prescription from Schlichting et al. (2015). These are impacts large and energetic enough to launch a shock wave through the target body and remove atmosphere from the opposite side of the body. For the isothermal atmospheres considered here this mass-loss is accounted for by an additional contribution to $\frac{m_{\rm atmloss}}{m_{\rm imp}}$ by

$$\frac{m_{\rm atmloss,GI}}{m_{\rm imp}} = \delta \frac{v_{\rm imp}}{v_{\rm esc}} \left[0.4 + 1.4x - 0.8x^2\right], \quad (8)$$

where $x \equiv \left(\frac{v_{\rm imp}}{v_{\rm esc}}\right)\left(\frac{m_{\rm imp}}{M_{\rm pl}}\right)$.

This effect is relevant only for the largest impactors, and given that we expect impacts by bodies larger than ∼100 km in size to be extremely rare on the outer satellites, this effect is not likely to contribute significantly to the atmosphere mass-loss predictions.

The fractional impactor mass accreted by the planet due to a single impact is given by

$$\frac{m_{\rm impacc}}{m_{\rm imp}} = \begin{cases} 1 & \eta \leq 10, \\ 1 - \chi_{\rm pr}(\eta) & 10 \leq \eta < 1000, \\ 1 - \chi_{\rm pr}(\eta = 1000) & 1000 < \eta, \end{cases} \quad (9)$$

where

$$\chi_{\rm pr}(\eta) = \min\left[0.07\left(\frac{\rho_{\rm tar}}{\rho_{\rm imp}}\right)\left(\frac{v_{\rm imp}}{v_{\rm esc}}\right)\left(\log_{10}(\eta) - 1\right), 1\right]. \quad (10)$$

The analytic prescriptions from Shuvalov (2009) are based on simulations of impactors with a range of sizes ($D = 1 - 30$ km), impact velocities ($v_{\rm imp} = 10 - 70$ km s^{-1}), and impactor densities ($\rho_{\rm imp} = 0.9, 2.8$ g cm^{-3}), undergoing cratering impacts on an Earth-like planet with atmosphere densities spanning $0.1 - 100$ times the present atmosphere mass of the Earth (0.85×10^{-6} M$_\oplus$). This results in a range of the erosional efficiency η (which is broadly analogous to the ratio of impactor energy to the escape velocity of the atmosphere) covering a range $\eta \approx 1 - 10^6$. We are extrapolating significantly to make use of this prescription on the outer moons, however this can be justified.

In the low energy impact regime the Shuvalov (2009) prescription for large η predicts total impactor accretion and negligible atmosphere mass-loss, as does the physically motivated model proposed by Melosh & Vickery (1989). When extrapolating the Shuvalov (2009) prescription into the 'airless limit', where the erosional efficiency becomes very large the atmosphere mass-loss necessarily becomes small and the accretional efficiency tends towards a constant value that may or may not be non-zero. The details of this prescription are discussed in detail in Section 2.2 but for now we note that a comparison performed in Sinclair et al. (2020) of this prescription to that presented by Cataldi et al. (2017) based on the experimental results of Housen & Holsapple (2011) found these two prescriptions to be in reasonable agreement. These prescriptions both predict finite impactor accretion at low atmosphere masses, which is also observed in the simulation results from Denman et al. (2020) and Leinhardt & Stewart (2012) which consider much more massive and therefore energetic impacts.

The Shuvalov (2009) impact prescription is dependent on the assumed atmosphere scale height through the erosional efficiency η. Any increase in the scale height, for example a hotter atmosphere temperature or change in the composition of the atmosphere that reduces the mean molecular weight, will decrease the value of η for a given impactor size and velocity. This results in a shift in the most efficient atmosphere-eroding impactor (that which has $\eta \sim 300$) to larger impactor sizes, and tends to favour increased impactor accretion. We do not include atmospheric chemistry or

alternative atmosphere temperatures in this paper, but note that they are important.

2.2 The airless limit and lower atmosphere mass limit

The behaviour of the atmosphere in the 'airless limit', where the atmosphere mass is very small compared to the impact vapour plume is significant when considering the thin atmospheres present on some of the outer satellites. We follow the approach used in Shuvalov (2009), such that this limit applies to impactors with $\eta > 1000$. In this limit $\chi_{\rm pr}$ is constant and the fractional impactor mass retained in a collision depends only on the impactor density and velocity. Typically, for impactors with comet-like densities, the accretion of material in the airless limit is relatively inefficient unless the impact velocity is low. In the extreme case of an initially bare rock target, this prescription allows growth of the atmosphere, with the efficiency depending on the density and velocity of the impactors.

It is helpful when considering extremely low atmosphere masses to quantify the point at which the atmosphere ceases to behave as a fluid. This does not address whether the prescriptions are valid all the way down to this limit, however the impactor accretion in the airless limit has been previously compared in Sinclair et al. (2020) to the atmosphere-less simulation results from Cataldi et al. (2017) and found to be in qualitative agreement. The fluid approximation relies on the mean free path, $\lambda = (\sqrt{2}n\sigma)^{-1}$ (determined by the number density of particles, n, and the collisional cross-section of the particles, σ) of a molecule or atom in the atmosphere being less than the typical length scale of the atmosphere. The atmosphere scale height, $H = \frac{kT}{\mu m_{\rm H} g}$, is independent of the atmosphere pressure and a good choice for a representative length scale.

Equating these two length scales gives a lower limit for the number density of $n_{\rm lim} = (\sqrt{2}\sigma H)^{-1}$, and therefore a lower limit on the surface pressure of $P_{\rm surf\,lim} = n_{\rm lim} kT$. Assuming an ideal gas, and provided that $m_{\rm atm}/M_{\rm tar} \ll 1$, the atmosphere mass is related to the atmosphere scale height, the target radius, ($R_{\rm tar}$), and the surface atmosphere density, ρ_0, by equation (3). Combining this with the surface pressure limit gives the following limit:

$$m_{\rm atm\,lim} \approx \frac{4\pi\mu m_{\rm H} R_{\rm tar}^2}{\sqrt{2}\sigma}. \tag{11}$$

This limit depends only on the atmosphere composition (through μ and σ) and the target body radius. For the oxygen molecules that make up the bulk of Europa, Ganymede, and the inferred component of Callisto, $\mu = 32$ and $\sigma_{\rm O_2} = 0.4$ nm^2. For CO_2, which is the observed component of Callisto's atmosphere $\mu = 44$ and $\sigma_{\rm CO_2} = 0.52$ nm^2 and for nitrogen as found in Titan's atmosphere $\mu = 28$ and $\sigma_{\rm N_2} = 0.43$ nm^2. Using these values, in combination with the appropriate target radii we can estimate the lower atmosphere mass limit for each of the outer satellites. This limit is lowest for Europa, at $\sim 5 \times 10^{-19}$ M$_\oplus$, and highest for Ganymede, at $\sim 1.4 \times 10^{-18}$ M$_\oplus$, relative to the masses of these moons these limits are between $\delta \sim (4-8) \times 10^{-17}$, respectively.

Below these limits, approximately $\delta = 10^{-16}$, the atmosphere can no longer be treated as a fluid, and the atmosphere should instead be considered a collision-less exosphere. This limit is just above the estimated mass for Europa's atmosphere, which is considered collisionless.

Whether or not an atmosphere can grow as the result of impacts on to an initially bare rock is dependent on the behaviour of impacts in this airless limit. In Section 2.4, we discus how this can (if criteria on the impactor density and velocity are met) result in the existence of a stable equilibrium atmosphere mass.

2.3 A simple model of impact-triggered outgassing

To calculate the volatile contribution as a result of impact-triggered outgassing, we construct a simple toy model based on the prescription from Kraus et al. (2011). This gives the relative mass of melted and vaporized target (moon) material ($m_{\rm m+v}$) for impacts into an icy surface,

$$\log_{10}\left(\frac{m_{\rm m+v}}{m_{\rm imp}}\right) = -0.53 + 0.0017T + 0.7\log_{10}(\sin\theta) - 0.46\phi + \frac{3}{2}(0.554 + 0.07\phi)\log_{10}\left(\frac{v_{\rm surf}^2}{E_m(\phi)}\right), \tag{12}$$

where $v_{\rm surf}$ is the velocity of the impactor at the surface of the planet, T is the atmospheric temperature, ϕ the surface porosity, θ the impact angle, and E_m the specific enthalpy of ice, H_2O(V). When including this prescription we assume a porosity of $\phi = 20$ per cent, a single impact angle of $\theta = \frac{\pi}{4}$, and constant temperature of $T = 100$ K. With these assumptions, the enthalpy $E_m(\phi, T) = E_m(\phi = 0.2, T = 100{\rm K}) = 7.85 \times 10^5$ J kg^{-1} (Kraus et al. 2011). Impacts with velocities below 8 km s^{-1} are predicted to produce no melting and thus contribute zero outgassed volatiles.

This prescription assumes impacts on to a surface with no atmosphere, and thus we also include, as done in Marounina et al. (2015), the expression for atmospheric drag from Svetsov (2007) to account for the potential deceleration of an impactor. This expression converts the impact velocity $v_{\rm imp}$ into a surface velocity $v_{\rm surf} = f v_{\rm imp}$, where

$$f = \exp\left[\frac{-\rho_0}{\rho_{\rm imp}}\left(\frac{1}{2}\frac{2H}{D} + \frac{4}{3}\left(\frac{2H}{D}\right)^2\sqrt{\frac{\rho_0}{\rho_{\rm imp}}} + 2\left(\frac{2H}{D}\right)^3\frac{\rho_0}{\rho_{\rm imp}}\right)\right]. \tag{13}$$

This results in both a general decrease in relative melted mass through the dependence of $m_{\rm m+v}$ on $v_{\rm surf}$ in equation (12) and a loss of melting from any impactors with $v_{\rm imp} \geq 8$ km s^{-1} but $v_{\rm surf} < 8$ km s^{-1}. The reduction in outgassing as a result of atmosphere drag becomes important only at atmosphere masses more massive than Titan's current atmosphere.

Combining the two expressions above allows calculation of the relative surface melt mass, which is then used in combination with the impactor mass ($m_{\rm imp}$) and initial surface volatile fraction ($x_{\rm v,targ} =$ 1 per cent) (Alibert & Mousis 2007; Waite et al. 2009) to calculate the mass of outgassed volatiles

$$m_{\rm outgas} = \begin{cases} m_{\rm imp}\left(\frac{m_{\rm m+v}}{m_{\rm imp}}\right)x_{\rm v,targ} & v_{\rm surf} \geq 8\ {\rm km\ s^{-1}}, \\ 0 & v_{\rm surf} < 8\ {\rm km\ s^{-1}}. \end{cases} \tag{14}$$

In order to account for the depletion of volatiles in the crust over time as a result of impact-triggered outgassing, we apply two limiting values to the outgassing prescription based on the available mass of volatiles in the crust. This first is a cap on the total mass of volatiles that a single impactor can release,

$$m_{\rm out,cap} = 2\pi\rho_{\rm surf} D^2(R_{\rm targ} - D)x_{\rm v,targ}. \tag{15}$$

This limit is analogous to the polar cap limit for atmosphere mass-loss given by equation (7) in that it limits the volume of the surface that can be vaporized to be less than the volume contained above the tangent plane, assuming the impactors penetrate to a depth of D. This cap applies only to the largest ($D \gtrsim 100$ km) impactors, limiting their volatile contribution to $\sim 10^{-8}$ M$_\oplus$ for the different moons.

For the volatile content, a range of $1-5$ per cent is reasonable for the material that makes up Titan, based on measurements of ammonia in the plumes from Enceladus (Waite et al. 2009) and models of the Saturnian nebula (Alibert & Mousis 2007). However Titan may be unique among the moons considered in this paper in its volatile-rich composition (Zahnle 2010). Clathrate structures can form on the Jovian moons, but unlike Titan are believed to form only a very thin surface layer ($\sim$10 m) (Hand et al. 2006).

We also place a limit on the total mass of volatiles contained in the crust that are available to be released by impacts by assuming that impacts are capable of outgassing at most the volatiles contained within a 20 km thick water ice ($\rho_{\rm surf} = 1$ g cm^{-3}) crust containing 1 per cent volatiles by mass (Alibert & Mousis 2007; Waite et al. 2009). This results in a total volatile mass limit that can physically be released by impact-triggered outgassing of 1.6×10^{-6} M$_\oplus$ for Titan, a ratio of $\delta \approx 7 \times 10^{-5}$ relative to the moon mass. This is preferable to assuming the observed crust thickness as a plausible depth, as volatiles deep in the crust may not be reached by the impactors. The equations describing the radius ($R_{\rm core}$) and depth ($D_{\rm core}$) of the isobaric core from Kraus et al. (2011) suggest that the largest, $D \approx 100$ km, impactors can penetrate to a depth of $\sim$200 km, deeper than the size of the typical crust. A subsurface ocean was shown to exist on Titan by Cassini (Iess et al. 2012). This raises the question of what happens when the melt penetrates to the subsurface ocean, but we leave consideration of this effect for future study. To estimate a depth to use in calculating the mass limit we consider instead the size of impactor expected to arrive in enough numbers to give good coverage of the entire surface of the moon. Taking as this size $\sim$10 km, of which a few hundred impactors are expected to arrive over the entire time period of the simulation, this predicts a depth of $17-19$ km, not dissimilar to our 20 km estimate.

The predicted behaviour of the atmosphere undergoing both atmospheric erosion and delivery due to impacts and impact-triggered outgassing is discussed in detail in Section 8.

2.4 An analytic approximation for the atmosphere stalling mass

Given the expressions above for the effect of a single impact, and assuming a plausible distribution of impactor properties it is possible to calculate the combined effect of a population of impactors. This is done by summing the individual contributions of a number of impactors, neglecting the stochastic nature of impacts and time evolution of the atmosphere and planet properties. This assumption means that while overall trends in atmosphere can be predicted, we are not aiming to predict the precise time-dependent behaviour of the atmosphere.

We start with the distribution of impactor properties as required by the numerical code with parameters as described in Section 2.5. Using the prescriptions for atmosphere mass removed by each impactor relative to the impactor mass $\left(\frac{m_{\rm atmloss}}{m_{\rm imp}}\right)_{i,j}$, and the impactor mass fraction retained after an impact $\left(\frac{m_{\rm impacc}}{m_{\rm imp}}\right)_{i,j}$ calculated using equations (4) and (9), the total atmosphere mass-loss caused by all impactors can then be calculated by summing over the size and velocity bins,

$$m_{\rm atmloss} = \sum_{i=1}^{N_{\rm size}} \sum_{j=1}^{N_{\rm vel}} \left[N_{i,j}(t) m_{\rm imp}(D_i, \rho) \left(\frac{m_{\rm atmloss}}{m_{\rm imp}} \right)_{i,j} \right], \tag{16}$$

where $N_{i,j}(t)$ is the number of impactors with size D_i and velocity v_j that arrive at time t. The total mass of impactor material accreted is then calculated in a similar fashion,

$$m_{\rm impacc} = \sum_{i=1}^{N_{\rm size}} \sum_{j=1}^{N_{\rm vel}} \left[N_{i,j}(t) m_{\rm imp}(D_i, \rho) \left(\frac{m_{\rm impacc}}{m_{\rm imp}} \right)_{i,j} \right]. \tag{17}$$

These values can be used to calculate the ratio of atmosphere mass gain to mass-loss rates,

$$f_{\rm v} = \frac{m_{\rm impacc} x_{\rm v}}{m_{\rm atmloss}}, \tag{18}$$

where $x_{\rm v}$ is the volatile fraction (the mass fraction of impacting material that will end up in the atmosphere as a gas rather than the solid surface after an impact) of the impacting population.

The value of $f_{\rm v}$ determines whether an atmosphere will grow (when $f_{\rm v}$ is greater than one) or whether it will deplete (when $f_{\rm v}$ is less than one). It therefore follows that atmospheres should remain unchanged in mass if $f_{\rm v} = 1$. This equilibrium atmosphere mass can be either stable or unstable, depending the exact dependence of $f_{\rm v}$ on atmosphere mass. If $f_{\rm v}$ increases with increasing atmosphere mass a small perturbation below the equilibrium leads to a value of $f_{\rm v} < 1$ and thus runaway depletion, equally, a small perturbation above the equilibrium mass leads to a value of $f_{\rm v} > 1$ and thus to runaway growth. This phenomenon is labelled as 'unstable' equilibrium for the rest of this paper. Conversely, if $f_{\rm v}$ decreases with increasing atmosphere mass then small perturbations away from the equilibrium will be corrected. This behaviour gives rise to the phenomenon of a characteristic 'stable' equilibrium atmosphere mass for a given population of impactors (Wyatt et al. 2020). In the following we will make use of the term 'stalling mass' to refer specifically to this stable equilibrium atmosphere mass.

The precise behaviour of $f_{\rm v}$ as a function of atmosphere mass in this prescription is a complex function of multiple impactor and target properties, but can be broadly grouped into five qualitative categories of behaviour:

(i) **Growth:** $f_{\rm v} > 1$ at all masses, typically resulting from slow, volatile-rich impacting populations that deliver large amounts of volatiles; the atmosphere always grows.

(ii) **Depletion:** $f_{\rm v} < 1$ at all masses, resulting from fast, low-density impactors with low accretion efficiency and erode significant atmosphere mass; the atmosphere always depletes.

(iii) **Stalling:** $f_{\rm v}$ decreases with increasing atmosphere mass, crossing one (where the atmosphere stalls) once – this typically results from mid-velocity, volatile-poor impactors that balance non-zero accretion in the airless limit with efficient erosion of the atmosphere when it exists.

(iv) **Low-mass stalling:** $f_{\rm v}$ first decreases then increases with increasing atmosphere mass, crossing one twice (so atmospheres that start below the second crossing will stall at the first, but those that start above the second crossing will undergo runaway growth) – this typically requires a truncated size distribution such that there are no large impactors to cause erosion of massive atmospheres.

(v) **Unstable stalling:** $f_{\rm v}$ increases with increasing atmosphere mass, crossing one once (where the atmosphere can stall but is unstable to small perturbations, which can result in runaway growth or runaway depletion) – this typically results from slower, low-density impactors that are accreted efficiently in massive atmospheres but can erode thin atmospheres.

These five behaviours are illustrated in Fig. 1, computed using five different combinations of impactor composition and velocity for impacts on to an Earth-like atmosphere ($m = 0.85 \times 10^{-6}$ M$_\oplus$, $T = 300$ K, $\mu = 28$) on an Earth-like planet. The properties of the planet, atmosphere, and impactor population can interact to produce

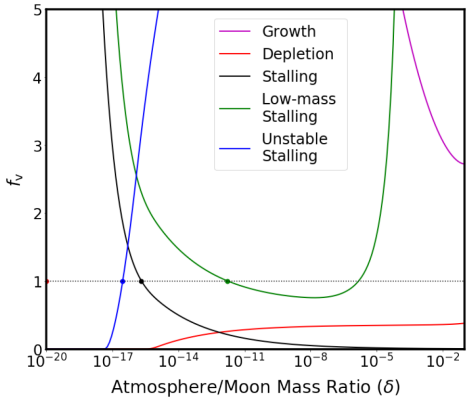

Figure 1. Five examples of the behaviour of f_v as a function of atmosphere mass, illustrating the different ways the atmosphere can (or cannot) reach the characteristic stalling mass. Regions of the line with f_v greater than one show atmosphere masses that will grow while those with f_v less than one will deplete.

any of the profiles shown, leading to a wide diversity of potential atmosphere behaviours. These computed curves consider only the cratering impact prescription of Shuvalov (2009) described in equations (4) and (9) (without the giant impact effects), and furthermore the impacting populations shown here are assumed to have a size distribution characterized by a single power-law and a single impact velocity. It should be noted that more complex behaviour is observed when more complex size and velocity distributions are considered, and when the effects of giant impacts, aerial bursts, and impactor fragmentation are included.

In comparison to the regimes of atmosphere evolution presented in fig. 2 in Zahnle et al. (1992), our $f_v > 1$ (growth) behaviour is analogous to their accumulative regime, while our $f_v < 1$ (depletion) is analogous to their erosion. However, while the results from Zahnle et al. (1992) also permit the existence of a single unstable equilibrium atmosphere mass, below which the atmosphere depletes and above which it grows, in our parametrization it is possible for the atmosphere to stall, something which is not possible in the framework of Zahnle et al. (1992).

The physically motivated 'snowplough' and 'bomb' impact prescriptions adopted in Zahnle et al. (1992) among other studies, distinguish between impacts that cause atmosphere mass-loss and deliver no volatiles and impacts that cause no atmosphere mass-loss but deliver the entirety of their volatiles to the atmosphere. Atmosphere mass-loss occurs if the impacts have mass above a critical value (the mass of the atmosphere contained in the tangent plane above the impact site, $m_{\rm tan} = \frac{H}{2R_{\rm targ}}$) and velocity above a critical value, $v_{\rm crit} = 2\sqrt{v_{\rm esc}^2 + 2L_{\rm vap}}$ (where $L_{\rm vap}$ is the enthalpy of vaporization for the target material). In the erosive regime atmospheres may survive if they are massive enough that the total impacting mass is insufficient to remove the entire atmosphere mass, otherwise as the atmosphere mass decreases, and thus the scale height falls, the critical impactor mass also decreases and impacts in general become more erosive and so the atmosphere is doomed to be entirely stripped. In their accumulative regime atmospheres evolve to a mass which is set by the total mass accreted. However this is different to our stalling mass, which is the atmosphere mass at which the rate of impact erosion balances the rate of volatile delivery and furthermore at which small deviations to the atmosphere mass are corrected back towards the equilibrium mass, because our stalling mass is independent of the total accreted mass.

While the results of Zahnle et al. (1992) would therefore suggest that the existence of a stable equilibrium stalling mass is impossible, alternative physically motivated atmosphere impact prescriptions do predict this behaviour. For example the 'cookie cutter' model from Walker (1986), in which atmosphere loss of heated material escaping along the vapour plume of the impactor is more important, allows a given impactor to efficiently remove atmosphere mass when an atmosphere is present but also contribute volatiles to an airless target. The key difference in these two physically motivated models is whether or not the potential of the impactor to remove volatiles from the atmosphere is decoupled from its ability to deliver volatiles as the atmosphere mass evolves.

For an atmosphere to exhibit the stalling behaviour it is necessary (but not necessarily sufficient) for $f_v \to \infty$ as $m \to 0$, i.e. a finite mass of impacting material must be accreted when no atmosphere is present (and there is no atmosphere mass to be lost). In the Zahnle et al. (1992) parametrization this is impossible unless the atmosphere always grows, for the reasons outlined above. However the Walker (1986) model and Cataldi et al. (2017), Zhu et al. (2019) and Shuvalov (2009) prescriptions do permit this behaviour. Specifically considering the Shuvalov (2009) prescription, in the airless limit ($\eta > 10^3$) the impactor mass retained is non-zero provided that (Wyatt et al. 2020)

$$\chi_{\rm pr} < 1$$

$$1 > 0.14 \frac{\rho_{\rm pl}}{\rho_{\rm imp}} \frac{v_{\rm imp}}{v_{\rm esc}}$$

$$\frac{v_{\rm imp}}{v_{\rm esc}} < 7.1 \frac{\rho_{\rm imp}}{\rho_{\rm pl}}, \tag{19}$$

i.e. as long as impactors are not excessively fast or low-density. Impacts above this derived velocity limit will always be erosive, and any atmosphere is therefore doomed to be stripped, analogous to the critical impact velocity in the 'snowplough' model. However, if impacts are below this velocity limit finite atmosphere mass gain but negligible atmosphere mass-loss is predicted on a bare target, and thus their ratio (f_v) becomes very large and an atmosphere is expected to grow. As the atmosphere mass increases, the potential for impact erosion to occur re-emerges. This atmosphere mass-loss can increase as the atmosphere mass available to be lost increases, however the impactor mass fraction accreted may not change significantly until the atmosphere is massive enough to cause significant drag on the impactor slowing it during its passage through the atmosphere. These effects can cause f_v to decrease as the atmosphere mass increases. If f_v remains above unity (typically when impacts are slow but volatile-rich) then the atmosphere will continue to grow indefinitely, leading to the runaway growth outcome described above.

However if impacts are faster, or more volatile-poor (but not so much that they fail to satisfy the inequality in equation 19) then f_v may cross unity, at the atmosphere stalling mass, and the stable stalling behaviour identified above may occur. If instead the inequality is not satisfied, and impacts remain erosive at high atmosphere masses (typically when they are fast), then the atmosphere experiences runaway erosion. Alternatively, as the atmosphere mass increases impacts may be slowed sufficiently in the atmosphere and result in net volatile delivery (typically when they are slower but low-density such that they can only be accreted in massive atmospheres). When the additional atmosphere mass-loss caused by giant impacts is included using the prescription from Schlichting et al. (2015) a second turning point can occur, leading to three atmosphere masses at which $f_v = 1$, two stable and one unstable. In this case, atmospheres initially below the unstable equilibrium mass will tend towards the

Table 1. Properties of a collection of outer Solar system satellites. The moon masses in $M_\oplus$ are Earth masses and the atmosphere masses are given as ratios to the moon mass ($\delta = \frac{m_{\rm atm}}{M_{\rm tar}}$). Separation is the orbital distance of the satellite to the host planet, and semimajor axis is the value of the host planet. * These atmosphere masses are calculated from pressure limits using equation (20).

Body	Mass ($M_\oplus$)	Density (g cm^{-3})	Separation ($\times 10^6$ km)	Semimajor Axis (au)	Atmosphere mass (δ)	Atmosphere MMW	Temperature (K)	Scale height (km)
Europa	0.00804	3.01	671.1	5.20	$(8.2 - 47.8) \times 10^{-17}$*	32	90	17.7
Ganymede	0.0248	1.94	1070.4	5.20	$(0.9 - 16.3) \times 10^{-17}$*	32	100	18.1
Callisto	0.0180	1.83	1882.7	5.20	$4.0 \times 10^{-16} - 2.0 \times 10^{-14}$*	44	125	28.2
Titan	0.0225	1.88	1221.9	9.58	6.7×10^{-5}	20	94	20.5

lower stalling mass, while those above it will tend towards the higher stalling mass.

2.5 A stochastic code to model atmosphere evolution

In order to more thoroughly investigate the potentially stochastic history of impacts on to the outer satellites we also make use of the statistical code of stochastic bombardment developed in Sinclair et al. (2020). This code as implemented in this paper is based on the impact prescriptions of Shuvalov (2009) and Schlichting et al. (2015), calculated according to equations (2) to (17), and was used to model the evolution of the Earth's atmosphere as it undergoes impacts. Given a specified population of impactors, this code will evolve the atmosphere through time, tracking the total atmosphere mass, planet mass, and atmosphere composition. In the results presented in Section 6, which does not include the contribution of impact-triggered outgassing, we make no modifications to the working of the code. Based on the fluid limit derived in Section 2.2 we adopt a lower atmosphere mass limit of 10^{-19} $M_\oplus$, below which the atmosphere mass is assumed to be negligible. As described in Section 2.2, an initially bare rock can either remain airless, or grow due to the delivery of volatiles by impacts in this airless limit regime.

A full description and testing of the code is carried out in Sinclair et al. (2020). Providing that sufficient impactor mass is delivered over the simulation time period, the analytic stalling mass as described in Section 2.4, which accounts for realistic impactor size and velocity distribution, is typically reached. However there are complexities to the atmospheric evolution as a result of both stochastic impactor arrival and the time evolution of the planet mass and atmosphere mass and composition that result in differences between the analytic prediction and the full numerical simulation results. The degree of stochastic variation observed between single iterations of the code assuming identical initial conditions depends on the nature of the atmosphere and impactors. Typically, smaller final atmosphere masses display greater variation in atmosphere mass due to stochastic effects.

A series of parameters describing the initial conditions of the planet and its atmosphere are required by the code. These are the planet semimajor axis ($a_{\rm pl}$) and stellar luminosity (L_*), which determine the atmospheric temperature, the target body mass ($M_{\rm tar}$), and bulk density ($\rho_{\rm tar}$). The initial atmosphere is described in terms of its mass (m_0) and bulk mean molecular weight (μ_0). The impactor population is described a bulk density (ρ), volatile fraction ($x_{\rm v}$), and mean molecular weight (μ). The size distribution is specified as the number fraction of impactors, in $N_{\rm size}$ log spaced size bins between a minimum ($D_{\rm min}$) and maximum size ($D_{\rm max}$). The number fraction of objects in the i-th size bin, with size D_i (and mass $m_{\rm imp}(D_i, \rho)$) is given by $f_{{\rm N},i}$. The impact velocity distribution is specified in a similar manner, with $N_{\rm vel}$ velocity bins log spaced between a minimum $v_{\rm min}$ and maximum $v_{\rm max}$ velocity. The number fraction of objects in the j-th velocity bin, with velocity v_j is given by $f_{{\rm v},j}$.

3 PROPERTIES OF THE OUTER SATELLITES

The properties of the four moons considered in this paper are summarized in Table 1.

When there is no observational atmosphere mass value to which we can compare the results of our models, we estimate an upper limit using observational surface pressure or column density ($n_{\rm col} = H\frac{P_{\rm surf}}{kT}$) limits through

$$m_{\rm atm} = \frac{3R_{\rm tar}P_{\rm surf}}{G\rho_{\rm tar}} = \frac{3R_{\rm tar}n_{\rm col}kT}{G\rho_{\rm tar}H}. \quad (20)$$

These lower limits are denoted by asterisks in Table 1. For Europa, Ganymede, and Callisto, the column densities have been inferred from observations and reported in the literature, while for Titan there are more direct estimates of the surface pressure that can be used to estimate the atmosphere mass. In the following, we describe the internal structure of these moons, which is important in determining the outcome of an impact, and describe the observationally inferred quantities from which we can calculate an estimate for the total atmosphere mass.

Ganymede, the largest Jovian moon, consists of an iron core, with a water ice and silicate mantle and potentially a subsurface internal ocean (Sohl et al. 2002). It is the largest object in the Solar system without a substantial atmosphere. Voyager was able to constrain the surface pressure to $<25 \times 10^{-12}$ bar (Broadfoot et al. 1981). The atmosphere is likely composed of O_2, as evidenced by *HST* observations of atomic oxygen air-glow and the spectroscopic detection of ozone and O_2 (Hall et al. 1998). The observed O_2 column density is $(0.3 - 5) \times 10^{14}$ cm^{-2} (Hall et al. 1998; Feldman et al. 2000), while the H_2 surface density is less than 10 per cent of this value and so ignored in the following calculation (Feldman et al. 2000). This column density, combined with the scale height and surface temperature from Table 1, gives an estimated surface pressure of $(0.02 - 0.40)$ μPa. This value can be converted into upper and lower limits for the estimated total atmosphere mass, which is shown in Table 1.

Callisto is the next largest moon of Jupiter and has a relatively low bulk density that implies a 50–50 rock-ice composition, with evidence for a silicate core and a subsurface ocean (Anderson et al. 2001). The surface is ancient and heavily cratered, with no evidence for tectonic or volcanic activity. The extremely thin inferred CO_2 atmosphere (~0.75 μbar) has a column density of 8×10^{14} cm^{-2} (Carlson 1999). However, evidence from the presence of a strong ionosphere implies a substantial molecular oxygen component, with a column density potentially as high as 4×10^{1} cm^{-2} (Liang et al. 2005; Cunningham et al. 2015). This results in an estimated surface

pressure of 0.73 μPa (36 μPa with the maximum inferred oxygen component).

Europa is the smallest of Jupiter's Galilean moons, with a majority silicate rock composition, a water ice crust, and potentially a metallic core (Kivelson, Khurana & Volwerk 2002). The surface is covered in cracks with few craters, which might be a result of the presence of a subsurface water ocean, evidenced by water vapour plumes. Europa's oxygen-dominated atmosphere is extremely thin, with a column density of O_2 observed to be $(2.4 - 14) \times 10^{14}$ cm^{-2} (Hall et al. 1998). This is frequently considered to be a collision-less exosphere[1] rather than a true atmosphere (Hall et al. 1995; Johnson et al. 2002). Using the scale height and surface temperature from Table 1, the estimated surface pressure is $(0.17 - 0.98)$ μPa. In comparison to the fluid limit derived in Section 2.2 the corresponding atmosphere mass estimate of Europa shown in Table 1 is very close to this lower limit.

Titan has a massive atmosphere composed of around 94 per cent N_2, with 5.6 per cent CH_3, 0.1 per cent H_2, and trace hydrocarbons (Catling & Kasting 2017). There is evidence for a methane cycle, with potential exchange between gas phases in the atmosphere and liquid and solid phases on the surface (Hörst 2017). The estimated surface pressure on Titan is 1.47×10^5 Pa (McKinnon & Kirk 2014). The scale height is 19.2 km and the atmospheric temperature is 88 K (Zebker et al. 2009). The estimated total atmosphere mass is thus 1.51×10^{-6} M$_\oplus$, and thus $\delta = 6.7 \times 10^{-5}$.

4 ASSUMED PROPERTIES OF THE NOMINAL IMPACTOR POPULATION

The small bodies in the Solar system that are responsible for impacts on to larger bodies can be split broadly into three populations based on their origin: comets from the trans-Neptunian disc, asteroids, and planetesimals left over after terrestrial planet formation. Impacts on to the outer satellites considered in this paper are expected to be dominated by comets, since this is the only population with an origin exterior to the satellites and so we consider only this population.

In the following results we consider first a nominal impactor population with properties as described below. This allows us to make a detailed investigation of the typical atmospheric stalling mass and its nature, and to isolate the effect of time-scales on these values. This nominal population is also used to investigate the stochastic nature of impacts using the numerical code. In the latter results we also consider the dependence of the typical stalling mass predictions on the assumptions we have made regarding the composition, size distribution, and velocity distribution of the impactors.

4.1 Impactor compositions

Our nominal impactor population is assumed to have a single homogeneous composition. Within our model for atmosphere evolution, this composition is specified by three parameters. These are the bulk density ($\rho_{\rm imp}$), the volatile fraction ($x_{\rm v}$), and mean molecular weight of the volatiles delivered by the impactor, $\mu_{\rm imp} = 28$ (Griffith & Zahnle 1995).

The impactor mean molecular weight has no effect on the predicted stalling mass, but does have a small but non-zero effect on the atmosphere evolution predicted by the numerical code because the atmosphere mass-loss and delivery fractions have a weak dependence on μ (i.e. the mean molecular weight of the atmosphere). If the mass of impact delivered volatiles is comparable to or greater than the atmosphere mass then the atmosphere is replaced by delivered material and the value of μ can change. This results in a minor change to the predicted atmosphere mass behaviour. Due to the relatively weak influence of this parameter we do not consider the effect of variation in it.

Comets display a wide degree of observed compositional diversity, and so we consider a range of potential values for these parameters. The density of comets has been estimated to lie between $0.3 - 1.2$ g cm^{-3}, and so we consider a range of bulk densities spanning $0.5 - 2.5$ g cm^{-3} to fully investigate the effect of this parameter (Festou, Keller & Weaver 2004). When considering the effect of variation in other parameters, we adopt a nominal comet composition with bulk density of 1.0 g cm^{-3}.

In our nominal case, we adopt an estimated volatile fraction for comets impacting the outer satellites to be 10 per cent (Griffith & Zahnle 1995). In reality the volatile content of the impactors is likely more complicated. There is evidence for significant compositional diversity among trans-Neptunian objects, and so we also consider a range of other potential volatile fractions in Section 7.2. These range from $2 - 50$ per cent to fully cover the range of potential outcomes.

The volatile fraction of a comet is not simply a property of the comet in isolation, as the species that are volatile and thus contribute mass to the atmosphere vary depending on the atmospheric temperature. For example Titan, the coldest moon that we consider, has an atmosphere temperature of 94 K, substantially lower than the estimated 125 K temperature of the atmosphere of Callisto. While we do not directly investigate this possibility, it could be that a different volatile fraction is more appropriate for Titan in comparison to Europa, Ganymede, and Callisto, as some volatiles may remain in their solid phases on colder moons.

4.2 Impact velocity distributions

The effect of an impact on the atmosphere depends sensitively on the impact velocity, and thus the choice of how to specify the distribution of impact velocities is important.

We follow the approach of Zahnle et al. (1992) to construct distributions of impact velocities on to the outer satellites based on dynamical arguments. A full derivation of these distributions is described in the appendix, Section A. We use these equations to calculate the impact velocity distributions for comets originating from three potential source regions. There are Uranus–Neptune planetesimals, Kuiper Belt objects, and Oort Cloud objects, which are assumed to have semimajor axes of $a = 25$, 50, or 20 000 au, respectively. The pericentre distributions are assumed to be uniform spanning $0.1 - 5.1$ au for the moons of Jupiter (Europa, Ganymede, and Callisto), and $5.3 - 9.4$ au for Saturn's moon Titan. The inclination distribution is assumed to be isotropically distributed between $i = 0$ and $i_{\rm max}$, with $i_{\rm max} = 10$ deg for the Uranus–Neptune planetesimals and Kuiper belt objects, and 180 deg for the Oort Cloud objects.

The impact velocities for the different source regions (Uranus–Neptune planetesimals, Kuiper Belt objects, and Oort Cloud objects) are shown in Fig. 2. From this plot it can be seen that the Kuiper Belt objects and Uranus–Neptune planetesimals show very similar distributions, while the Oort cloud objects are typically faster. This results from the higher inclinations of the Oort cloud objects relative to the plane of the planets. The Kuiper belt population is expected to dominate the delivery of material to the outer moons in comparison to the Uranus–Neptune planetesimals and Oort cloud objects and so we adopt the Zahnle et al. (1992) calculation for impacts from this region

[1] gravitationally bound material that does not behave as a fluid

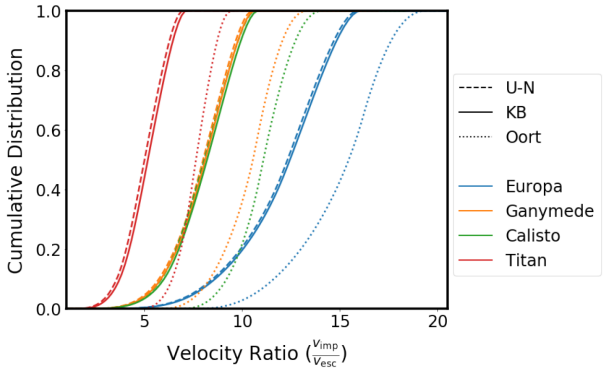

Figure 2. The cumulative distribution of impact velocities on to the four moons by impactors from three different source regions, calculated according to the Zahnle et al. (1992) method as described in the text. Objects from the Oort cloud ($a = 20\,000$ au, $i = 0 - 180$ deg isotropic), Kuiper belt (our nominal population, $a = 50$, $0 < i < 10$ deg), and Uranus–Neptune planetesimals ($a = 25$, $0 < i < 10$ deg) are shown by different line styles. Each distribution is shown as a ratio of impact velocity to the escape velocity of the moon.

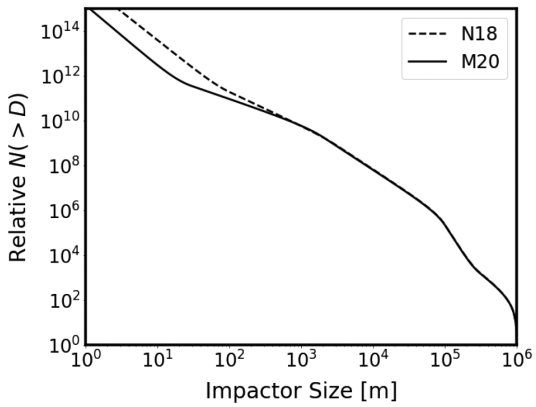

Figure 3. The cumulative size distribution normalized such that there is one object with $D \geq 1000$ km in the size distribution. The nominal (Morbidelli et al. 2021) size distribution is shown as a solid line with a slightly different (Nesvorný et al. 2018) size distribution that is used for investigating the sensitivity of our results to the assumed size distribution shown as a dashed line.

as our nominal distribution of impactor velocities unless otherwise specified. The difference in predicted atmosphere outcomes resulting from the three different source regions is investigated in Section 7.4.

4.3 Impactor size distribution

4.3.1 The slope of the impactor size distribution

Our nominal size distribution is a piecewise combination of power laws (specified by α, the power-law index of a differential power-law distribution, such that the number of objects with sizes between D and $D + \mathrm{d}D$ is $\mathrm{d}N \propto D^{-\alpha}\mathrm{d}D$), based on the observed trans-Neptunian object size distribution from Morbidelli et al. (2021). This distribution is illustrated in the top panel of Fig. 3. This distribution is similar to an $\alpha \sim 3.1$ differential power-law size frequency distribution, with values of α between 2.5 and 3.7 for impactors up to 100 km and relatively fewer larger impactors. We also consider an alternative size distribution for the trans-Neptunian objects from Nesvorný et al. (2018) (also illustrated in Fig. 3) to investigate the sensitivity of our results to the assumed size distribution. This is similar for the largest objects, which contain most of the mass, but differs in the number of sub-km objects, of which there are relatively fewer in the Morbidelli et al. (2021) distribution. These two size distributions represent a realistic range of potential size distributions, and so are useful in constraining the influence of this parameter on our predicted atmosphere behaviour. These results are discussed in Section 7.3.

4.3.2 Upper and lower impactor size limits

We can also ask how the predicted stalling masses depend on the extent of the assumed size distribution of the impactors. The choice for the lower size limit is not a physical limit, since collisions will populate the size distribution to arbitrarily low sizes. At small enough values of the erosional efficiency parameter η (small enough sizes) the effect of the impactor on the atmosphere becomes negligible, however η also depends on atmosphere mass and thus the size below which impacts can be neglected decreases as the atmosphere mass decreases. Based on convergence testing using a realistic range of impactor and target properties we find that impactors smaller than 0.01 m typically have no impact on the atmosphere behaviour for atmosphere masses above the fluid limit and thus we choose a conservative lower limit of 100 μm.

The upper size limit is more complicated, since the largest impactor to have collided with a moon is determined by a combination of stochastic effects, the slope of the size distribution, and the assumed impact rates. The largest impactor sizes are typically unlikely to be sampled over the age of the Solar system given the total masses considered, that is $N(>D) \leq 1$ for a size D below the upper limit of the sampled distribution, and thus including their effect in the analytic prediction will lead to inaccurate predictions. Unlike the slope and the lower size limit, this parameter is treated differently in the numerical code compared to the analytic prediction. In the numerical code, the maximum impactor size is determined by the stochastic sampling of the impactors from their parent population. In the analytic approximation, it must be explicitly set to avoid including what could be a significant contribution to atmosphere erosion or volatile delivery by a very unlikely impactor. To do this, we calculate the cumulative impactor numbers $N(>D)$ and define the nominal maximum impactor size for each impactor population to be the size at which $N(>D_{\mathrm{max}}) = 1$ once the total mass of impacting material has been delivered, assuming the nominal impactor density of 1 g cm^{-3}. The assumed impact flux and total impacting mass choices are discussed in Section 4.4. The influence of the largest sampled impactor size on the predicted atmosphere stalling mass is explored in more detail in Section 5.2.

4.4 Impact rates and total impacting mass

The impact fluxes, which give the total number of impacts of all velocities on to the outer satellites as a function of time, are important when considering the absolute time evolution of the atmosphere. The analytically predicted stalling mass is not dependent on the impact flux, however the time taken to reach this stalling mass does depend on the impact flux through the total mass of impacting material. We estimate the impact fluxes and total impacting mass using the ratio of impacts at all velocities by ecliptic comets (assumed to be the dominant source of impactors) on to the outer moons relative to Jupiter at the present epoch, from the Monte Carlo calculations carried out in Zahnle et al. (2003). Taking the current rate of cometary

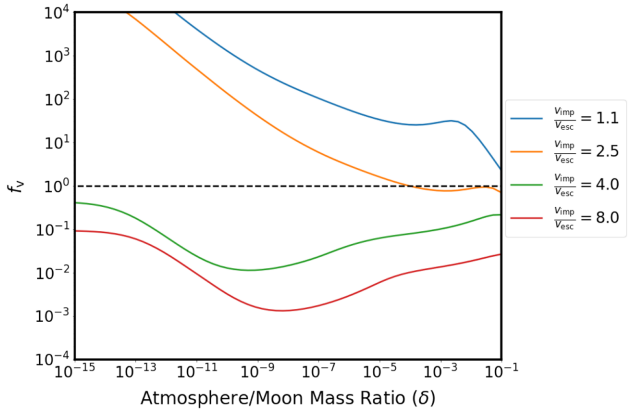

Figure 4. The calculated values of the ratio of atmosphere mass gain to mass-loss (f_v) as a function of atmosphere mass for a representative range of impact velocities. These results are shown for a single representative impactor density (1 g cm^{-3}) and for impacts on to Titan, with the line colour illustrating the impact velocity.

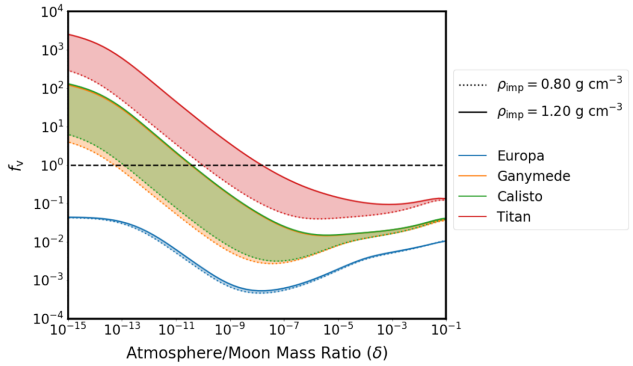

Figure 5. The calculated values of the ratio of atmosphere mass gain to mass-loss (f_v) as a function of atmosphere mass summed over a realistic distribution of impact velocities. These results are shown for a range of impactor densities illustrated by the line style given in the caption, with the range between these densities shown as a shaded region. Each moon is shown by a different line and shading colour.

impactors with all sizes with $D > 1.5$ km on to Jupiter to be $\dot{N}(D > 1.5\text{km}) \approx 0.005\,\text{yr}^{-1}$ from the same work, the same rate on to each of the four outer satellites can be calculated. These rates imply a total mass impacting the outer moons over the last Gyr of around $1.4 - 3 \times 10^{-8}$ M$_\oplus$, highest for Ganymede and lowest for Titan.

This current rate is likely significantly lower than the rate of bombardment experienced in the early history of the Solar system, and so we attempt to correct for this by estimating the decay in impact flux. To do this we use a model fit to calculated comet impacts on to Mars from data based on the simulations of Nesvorný et al. (2017) over the first Gyr after Solar system formation. This results in a total impacting mass over the entire history of the Solar system (between just after the assumed time of the giant planet instability, $t_0 = 6$ Myr Nesvorný, Vokrouhlický & Morbidelli 2013, and the present day) that is 650 times more massive than the estimate of the last billion years, $\sim 10^{-5}$ M$_\oplus$ on to each moon.

The largest object to impact each moon should, using this approach, have a size $D_{\max} = 166 - 197$ km. It should be noted that impactors of this size are rare, and likely to have occurred early when the impact flux was highest. The current impact rate over the past 2 Gyr predicts a maximum impactor size of $D_{\max} = 44$ km on Ganymede, in agreement with the expected size of the comet required to create the largest impact crater, Gilgamesh (Zahnle et al. 2003). It is possible that our total impacting mass estimates are too high, however we do not consider variation in this parameter as it influences our predicted stalling masses only indirectly through the size of the largest impactor used in the analytical calculation, and the time-scale on which the predicted stalling mass is reached, which is investigated in Section 5.2. When considering variation in the impactor density we assume that these maximum impactor sizes are held constant and vary only the impactor density (and thus total impacting mass) to isolate the influence of this parameter.

Given the inherent uncertainty in the specific details of the impact chronologies, and the insensitivity of the final atmospheres to the absolute times at which the impacts arrive we present the results from the numerical code as functions of the mass that has impacted each moon (increasing from zero to the total mass). Due to the assumed size distribution of impactors, most mass is contained in the largest bodies, and thus since the analytic stalling mass prediction is sensitive to this largest impactor size, it therefore depends on the time-scale over which the evolution of the atmosphere is considered. This phenomenon is explored in detail in Section 5.2, where we demonstrate that while the impact flux rates influence the degree of stochasticity expected from the numerical results, the predictions for the atmosphere stalling mass are unchanged.

5 ANALYTIC PREDICTIONS FOR THE ATMOSPHERE STALLING MASS

We can now calculate the analytic stalling mass described in Section 2.4. This is done for all four outer moons, focusing on Titan when detail is needed, assuming the nominal impactor population described above. We first consider the maximum impactor size that should be used in these calculations, that is set by the estimated total impacting mass, as described in Section 4.3, before discussing how the time-scale over which the impactors are sampled should be considered when calculating the predicted stalling mass for the atmosphere.

5.1 Stalling mass predictions due to the nominal impactor population

The first step is the calculation of f_v as a function of impact velocity, impactor density, and atmosphere mass for each of the four outer satellites, using equation (18). This requires summing over the size distribution of impactors up to the maximum impactor size, defined as $N(> D_{\max}) = 1$ as discussed in Section 4.3.2, over a time-scale of 4.5 Gyr to consider the long-term evolution of the atmospheres. An example of the kind of $f_v(m_{\text{atm}})$ curves produced for impacts with a range of velocities on to Titan are shown in Fig. 4. Where these lines cross one on the y-axis (if they do so) illustrate atmosphere masses at which the rate of impact delivered volatile gain matches impact driven atmosphere loss and there is an equilibrium, as described in Section 2.4.

However, considering the effect of a single impact velocity in isolation is not physically realistic, since in reality impacts will occur with a range of impact velocities. The effect of a realistic velocity distribution can be seen by calculating the weighted average of f_v over all impactor velocities. These averaged curves are shown for a representative span of impactor densities in Fig. 5. Lower density

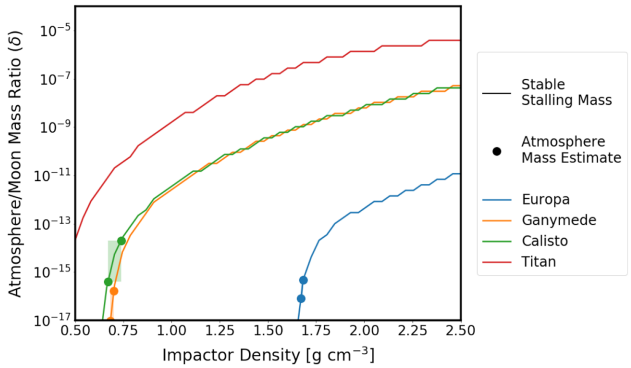

Figure 6. The stalling masses predicted for each of the moons summing the contributions to f_v using a realistic velocity distribution. The results for each of the different moons is shown by a different line colour, with a shaded rectangle between two markers indicating the region of parameter space in which the predicted stalling mass is in agreement with the estimated atmosphere mass limits given in Table 1.

impactors can be seen to cross one at lower atmosphere masses for all moons. The atmosphere mass at which $f_v = 1$ is highest for Titan, followed by Callisto and Ganymede (which are almost indistinguishable). Europa has a value of $f_v < 1$ at all atmosphere masses, suggesting that impacts are never capable of growing an atmosphere on this moon. Fig. 5 also illustrates the necessity of averaging f_v over a distribution of impactor velocities, rather than simply adopting a single representative velocity, since these resultant curves are not well represented by any of the lines from Fig. 4.

We can now calculate the stalling mass (if it exists) as a function of impactor density by locating the atmosphere mass at which $f_v = 1$ for each of the four outer satellites. These values are illustrated in Fig. 6. Comparing these results to the actual atmosphere mass ratios on each of these bodies estimated from observations we find our results recreate the trends in relative atmosphere masses. For Europa (which has essentially no atmosphere) we predict runaway atmosphere depletion for all but the highest density impactors. The pattern of increasing atmosphere masses from Ganymede to Callisto seen in the observations is matched by our results, although no single impactor density results in simultaneous matching of all the observed masses. For example, an assumed impactor density of 1 g cm^{-3} is reasonable for Europa but overestimates the observed atmosphere masses of Callisto and Ganymede by more than an order of magnitude. The atmospheres of these moons are not impact generated, and so we do not expect to match them precisely. Instead our results suggest that impacts would not result in the accumulation of volatiles on these moons, which would be in conflict with the observations. While we do predict a higher atmosphere stalling mass ratio for Titan than the other moons at all impactor densities ($\delta = 1.4 \times 10^{-9}$ for $\rho_{imp} =$ 1 g cm^{-3}), the actual atmosphere mass ratio of 6.5×10^{-5} is four to five orders of magnitude higher than our predicted stalling mass. The potential solution to this discrepancy, impact-triggered outgassing, is discussed in Section 8.

5.2 Consideration of the time-scales taken to reach the analytic stalling mass

The analytic prediction for the stalling mass calculated as described in Section 2.4 is a useful quantity when considering the long-term evolution of a small body's atmosphere. However, it does not on its own address the feasibility of reaching the predicted stalling mass

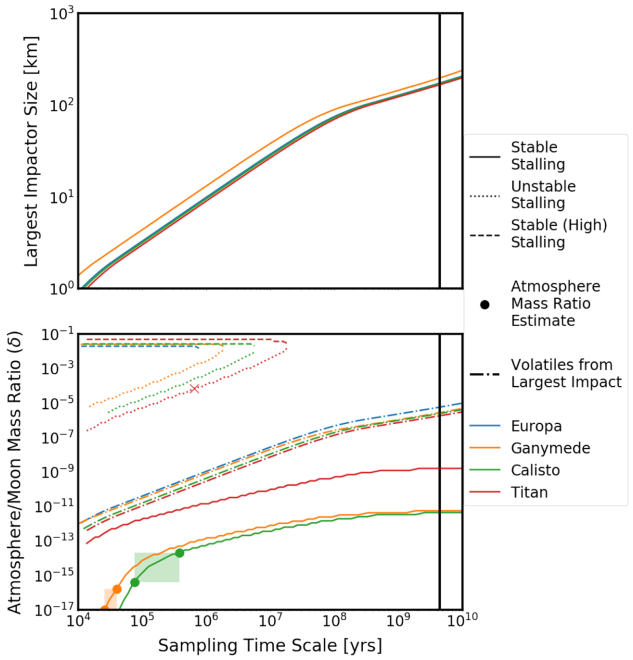

Figure 7. The top panel shows the dependence of the largest impactor size (D_{lim}) that is expected to have impacted the moons on the time-scale over which evolution of the atmosphere is considered, calculated from the impact fluxes as described in the text. The atmosphere stalling masses calculated for these largest impactor sizes are shown in the bottom panel as a function of the time-scale. The lower stable stalling mass is shown by a solid line, the larger stable stalling mass by a dashed line, and the unstable equilibrium mass that separates the two by a dotted line, with the line colour illustrating the moon for which the values are calculated. The location on the lines of stalling mass that are in agreement with the estimated range of observed atmosphere masses from Table 1 are shown by shaded rectangles between two markers, with the colour again illustrating the moon. The mass of volatiles contained in the largest impactor expected to be sampled in the time-scale is shown by a dash-dotted line in the same colour. The entire time period of the simulations ($\tau_{sample} = 4.5$ Gyr) is shown by vertical black lines on both panels, from which the maximum impactor size (described in Section 4.3) and nominal stalling mass predictions (described in Section 5.1) can be inferred.

within the age of the system. The stalling mass is independent of the mass accretion rate, but in the analytic calculation it does depend on the size of the largest body expected to impact the moon.

The adopted size distribution and mass accretion rates described in Sections 4.3 and 4.4 together determine the size of the largest impactor, D_{lim}, sampled over a given time-scale, τ_{sample}, i.e. the impactor size at which one impactor of this size or larger is expected to arrive in this time period. These two quantities are related through

$$\int_0^{\tau_{sample}(D_{lim})} \dot{N}(> D_{lim})\, dt = 1. \quad (21)$$

This relationship is illustrated for each of the four outer moons in the top panel of Fig. 7. Over the entire time-span considered, 4.5 Gyr, once the moons have undergone the expected total bombardment, this largest impactor size is equal to the maximum impactor size discussed in Section 4.3.2 (i.e. $D_{lim}(\tau_{sample} = 4.5\text{Gyr}) = D_{max} \approx$ 170 km). On shorter time-scales the size of the largest sampled impactor decreases, and considering the effect of this truncated size distribution on the atmosphere, keeping all other impactor and moon properties constant, results in a lower value for the predicted atmosphere stalling mass, $m_{stall}(D_{lim})$, as shown for each of the four outer moons in the bottom panel of Fig. 7.

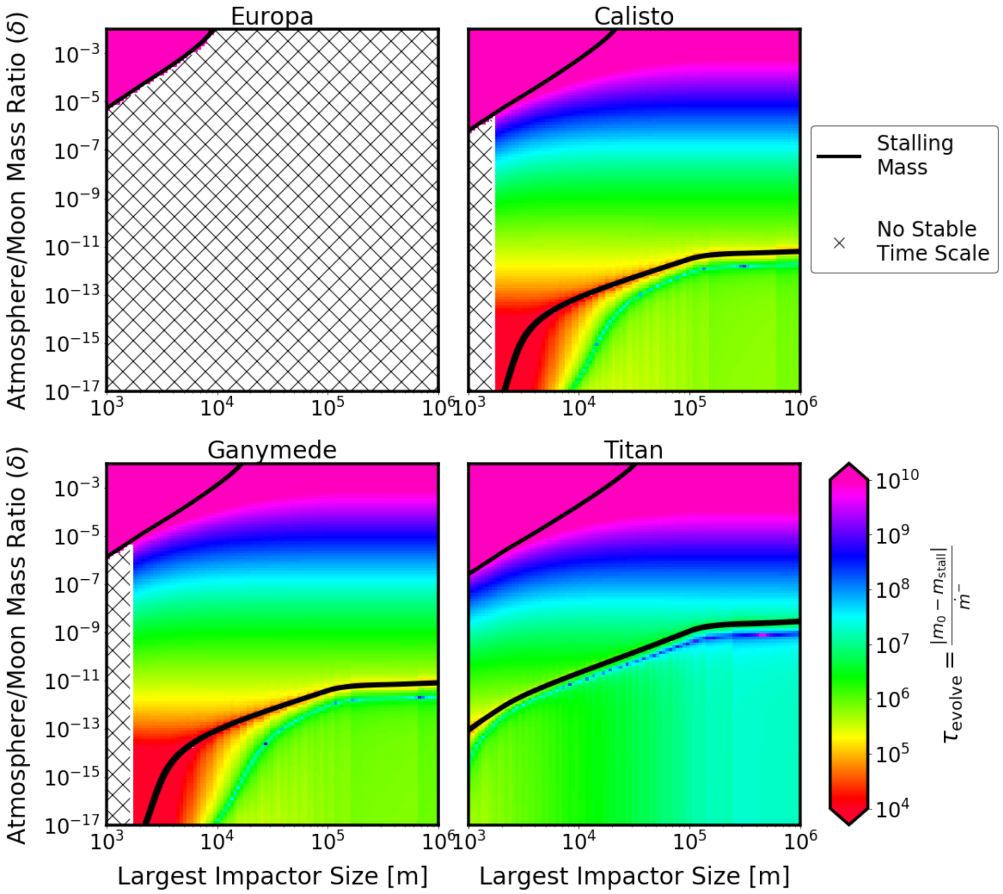

Figure 8. The value of the evolution time-scale τ_{evolve} (defined in equation 22) as a function of maximum impactor size and atmosphere mass. The locations of the equilibrium atmosphere masses are shown by thick black lines. When the largest impactor size is small there are multiple equilibrium stalling masses, two stable and one unstable. The evolution time-scale shows a sharp increase at atmosphere masses just below the stalling mass due to competing numerator and denominator in equation (22) both tending towards zero as the atmosphere mass tends towards the stalling mass. Initial atmospheres less massive than the middle (unstable) equilibrium mass will tend towards the lower stalling mass while those more massive than the unstable equilibrium mass will tend towards the higher stalling mass. Where the plots are marked by black hatching there is no accessible stable stalling mass and the atmosphere is expected to undergo runaway depletion.

At small maximum impactor sizes (below a few 10s km) a new phenomenon emerges, that of multiple equilibrium atmosphere masses (resulting from a $f_v(m_{atm})$ curve that crosses one multiple times). This results in the typical stable stalling mass remaining at low atmosphere masses, but an unstable equilibrium point at some higher atmosphere mass. An atmosphere mass below this unstable equilibrium point should undergo erosion to the stable atmosphere mass, however if some stochastic event were to increase the atmosphere mass above this unstable equilibrium point, the atmosphere should grow until it reaches the second, higher, stable atmosphere stalling mass. This effect is interesting, but the second, high mass stalling atmosphere state is never accessible as a result of impacts. This would require the occurrence of a single stochastic event that can deliver enough atmosphere mass to jump from the bottom stable atmosphere mass to above the unstable equilibrium, which requires the delivery of 10^{-8} $M_\oplus$ in volatiles in a single event, which assuming the nominal impactor properties corresponds to the volatiles contained in a single 110 km diameter object. This size of object is expected to impact the outer moons, however the accretion efficiency of these large bodies is low, and so either a substantially more massive impactor (which would be very rare) or an extremely slow impact (which is also rare) is required to deliver this mass in a single event. For this reason, in the following we consider only the lower stable atmosphere stalling masses.

To understand whether the predicted atmosphere stalling mass is a realistic prediction for the actual behaviour of the atmosphere we need to consider first whether the population of impacting bodies is capable of eroding or growing an initial atmosphere up or down to the final stalling mass. In order to answer this first question, we define an atmosphere evolution time-scale,

$$\tau_{evolve} = \frac{|m_0 - m_{stall}(D_{lim})|}{\dot{m}(m_0, D_{lim})}, \quad (22)$$

where m_0 is the initial atmosphere mass and $\dot{m}(m_0, D_{lim})$ is the initial rate of atmosphere mass change for an atmosphere with mass m_0 impacted by objects up to a largest size D_{lim}. This time-scale represents the time taken for an atmosphere to evolve from its initial mass to the stalling mass $m_{stall}(D_{lim})$, ignoring the fact that $\dot{m}$ depends on the atmosphere mass (and is zero at the stalling mass) and so will change as the atmosphere evolves towards the stalling mass.

The dependence of the time-scale on the atmosphere mass and the size of the largest impactor is illustrated in Fig. 8. The stable stalling masses and unstable equilibrium masses are also illustrated on this plot, and no time-scale is shown when no accessible stable stalling mass exists. The evolution time-scale shows a sharp increase at atmosphere masses slightly lower than the stalling mass value, as both the numerator and denominator of equation (22) tend towards zero at slightly different rates. These time-scales imply that even initially

bare moons could grow to the stalling mass over the full time span of the simulation (once they have undergone the bombardment expected over the age of the Solar system), a result that is supported by the observation from Fig. 7 that at all time-scales the volatiles contained in the largest sampled impactor are greater than the predicted stalling mass suggesting that growth to this stalling mass from an initial atmosphere mass less than the stalling mass is a realistic proposition. The results shown in Fig. 8 also suggest that initial atmosphere masses of approximately less than 10^{-7} $M_\oplus$ can be eroded to the stalling mass within this time period. This upper atmosphere mass limit is lowest for Titan, which has the longest evolution time-scales, followed by the Jovian moons. Despite this, the time taken for larger initial atmosphere masses to deplete to the stable stalling mass can be very long, suggesting that impacts alone are incapable of eroding massive primordial atmospheres to the current observed levels on these moons.

The second question we can ask is whether the behaviour of the atmosphere at the stalling mass is expected to be smooth or dominated by stochasticity. To address this question, we need to consider the relationship between the evolution time-scale defined in equation (22) and the stalling mass. We do this here using Titan and Ganymede as example cases.

For Titan, the results shown in Fig. 8 demonstrate that, provided the initial atmosphere mass is not so massive that it cannot be eroded within the time span of the simulation, stalling masses are typically reached in around 1–10 Myr, with this time largely insensitive to the size of the largest impactor. From Fig. 7, it can be seen that in this time-scale objects around 10–20 km are expected to be accreted, leading to a predicted atmosphere stalling mass to moon mass ratio of $\delta \sim 4 \times 10^{-11}$. This is lower than the value of 1.40×10^{-9} predicted for the full distribution of objects up to $D_{\rm max} = 170$ km expected over the entire time span considered. However, larger objects between 10 and 170 km in size are also impacting the moon in a stochastic fashion. These impacts deliver substantial volatile masses resulting in atmospheric growth, but this is rapidly followed by depletion back to $\delta \sim 4 \times 10^{-11}$ over a time-scale of 1–10 Myr due to the continuous accretion of smaller objects. Over the full 4.5 Gyr time span of the simulation we therefore expect the atmosphere to moon mass ratio to vary stochastically between $\delta \sim 4 \times 10^{-11}$ and approximately 10^{-7} (the maximum mass in volatiles that could be delivered by a single impact by the largest body expected over the full simulation).[2]

As a comparison, we can also consider Ganymede, which is predicted to have a much lower atmosphere stalling mass-to-moon mass ratio than Titan. In this case Fig. 8 shows that the stalling mass is typically reached on a shorter time-scale, $\sim 0.1 - 1$ Myr, which from Fig. 7 can be seen to correspond to the accretion of ∼2−5 km sized objects and thus a predicted atmosphere stalling mass ratio of $\delta \sim 10^{-16}$, close to the fluid limit. We therefore would expect the atmosphere mass to vary stochastically between this value and a few $\times$ 10^{-8}.[3] This is substantially more stochastic variation than predicted for Titan, suggesting that lower predicted atmosphere stalling masses would be expected to show more stochastic variation in the numerical code results. These predictions are compared to the results of the numerical code in Section 6.3.

[2]Assuming an accretion efficiency of 10 per cent for a $D = 170$ km comet ($\rho_{\rm imp} = 1$ g cm^{-3}, $p_{\rm v} = 0.1$) which contains $\sim 3 \times 10^{-8} M_\oplus$ in volatiles.
[3]Slightly lower than the upper limit calculated for Titan due to the lower accretion efficiency expected on the Jovian moons

5.3 The effect on the atmosphere behaviour of the current impact flux

The discussion above cannot directly be applied to the present day evolution of the atmospheres of the moons, as we are assuming here the constant impact rate described in Section 4.4, which is an average rate calculated over the entire age of the Solar system. For this reason the absolute times given are not directly able to be translated into real times. However the general arguments made regarding the comparison of the two time-scales are applicable regardless of the impact rate, since for a constant value of $D_{\rm lim}$, both time-scales scale with the impact rate in the same way. The true impact rate at the current time is lower than our assumed average rate (discussed in Section 4.4), by a factor of approximately 145. This is equivalent to shifting the lines on the top panel of Fig. 7 to the right by a factor of 145, meaning that in a given time-scale the largest impactor expected to arrive will be smaller. The specific factor by which the size of the largest impactor will decrease depends on the slope of the size distribution, which is not constant, but in general it is within an order of magnitude, between 1 and 10. Since the stalling mass is dependent only on the size of this largest impactor, not the impact rate, this will also shift the lines in the bottom panel of Fig. 7 to the right by the same factor of 145, decreasing the predicted stalling mass for a given time-scale. When considering the evolution time-scale shown in Fig. 8, the current impact rate gives time-scales that are also a factor of 145 higher. We can again use Titan and Ganymede as example cases to consider how this influences the predicted atmosphere stalling mass and stochastic behaviour.

We infer from Fig. 8 that, for Titan, the stalling mass is now expected to be reached in around 100 Myr to 1 Gyr. However because the sampling time-scale has increased by the same factor, the stalling mass to which the atmosphere evolves towards is still determined by the accretion of objects up to the same size as before, 10–20 km, and thus this predicted stalling mass ratio ($\delta \sim 4 \times 10^{-11}$) is unchanged. As discussed above, the atmosphere is perturbed away from this equilibrium by the stochastic accretion of objects larger than 10–20 km, and therefore the lower bombardment rate results in decreasing frequency of those impacts. This means that the maximum impactor size expected to arrive over the full 4.5 Gyr (if the bombardment rate was constant at the current rate throughout) would be reduced from 170 to 43 km. This means that the stochastic variation in the atmosphere mass is no longer likely to peak at a few $\times 10^{-9}$ $M_\oplus$ ($\delta \sim 10^{-7}$) but instead at approximately 10^{-10} $M_\oplus$, which is the mass of volatiles that could be delivered by this largest impactor. The same conclusions are reached for Ganymede and the other three moons; the time-scales are longer and so evolution is slower but the stalling mass to which the atmosphere is predicted to tend towards is unchanged. The distribution of atmosphere masses above this caused by the stochastic accretion of the largest bodies is not expected to reach such large atmosphere masses as a few 10^{-9} $M_\oplus$, due to the lower rate of impacts by the larger bodies that deliver significant volatile masses to the outer moons.

6 RESULTS FROM THE NUMERICAL CODE FOR ATMOSPHERE EVOLUTION

6.1 The evolution of Titan's atmosphere in detail

We first consider the evolution of Titan's atmosphere under bombardment by the nominal population of impactors, using the numerical code described in Section 2.5, without considering the effect of impact-triggered outgassing. This allows us to investigate the

effects of stochasticity in detail, and investigate the behaviour of atmospheres with different initial atmosphere masses. The code is run a total of ten times for each of four different initial atmosphere masses spanning $10^{-15} - 10^{-6}$ $M_\oplus$ ($\delta = 4 \times 10^{-14} - 4 \times 10^{-5}$) and a uniform impact rate, adopting the nominal impactor properties as described in Section 4. Impactors are sampled stochastically from the size distribution as described in Section 4.3, which results in a typical largest sampled impactor size for Titan of ∼170 km. As discussed in Section 4.4 we adopt a time-independent impact flux and thus the results are presented as functions of impacting mass not time. These results should be interpreted bearing in mind that the majority of impacts are expected to occur early.

The resulting atmosphere mass evolution is illustrated in the left-hand panel in the fourth row in Fig. 9. The evolution of the ratio of atmosphere to planet masses shows two main features. First, there exists a significant amount of stochastic variation between iterations and within the same run, as predicted in Section 5.2. Secondly, there is a tendency for the atmospheres with initial masses $\leq 10^{-7}$ $M_\oplus$ to converge to the same (stochastic) behaviour after a period of impacts. The atmosphere that starts with a higher initial atmosphere mass, similar to the current value, depletes slightly but is too massive for the assumed total mass of impactors to erode a significant fraction of its initial mass.

We can compare the stochastically varying atmosphere masses recorded in the numerical results to the stalling mass predicted by the analytic arguments by considering the median and mean atmosphere mass over a suitably long period. The right-hand panel in the fourth row in Fig. 9 shows the histogram of atmosphere masses sampled at approximately 1100 evenly spaced intervals for each iteration of the code over the delivery of the final 20 per cent of the total impacting mass. A comparison of these results to the analytically predicted stalling mass for all of the moons is discussed in Section 6.3 below.

6.2 Results from the numerical code for all moons

The numerical atmosphere evolution results for the other three Moons are shown in the left-hand column in Fig. 9. Unlike in the case of Titan, a 10^{-6} $M_\oplus$ initial mass atmosphere cannot be maintained for the full span of the simulations on any other moon. As was seen for lower initial atmosphere masses on Titan, the atmospheres on all other moons rapidly forget their initial mass and show a high degree of stochastic variation within and between iterations of the code. Europa is never recorded with an atmosphere mass higher than the lower atmosphere mass limit implemented in the code after the initial period of atmosphere erosion.

The distribution of sampled atmosphere masses over the impacts by the final 20 per cent of the total impacting mass for each simulation (allowing the initial atmosphere mass to be 'forgotten') are shown for each of the four initial atmosphere masses in the right-hand column of Fig. 9. These results show similar convergence of the atmosphere mass, however the median final atmosphere mass varies between the different moons. Ganymede and Callisto show similar, lower mass, distributions of final atmosphere masses. In all cases there is an artificial peak in the distribution at the atmosphere to planet mass ratio bin corresponding to the lower limit implemented in the numerical code.

6.3 Comparison of the numerical code results to the analytic predictions

We now have results from the numerical code that can be compared to the analytic predictions for the stalling mass from Section 5.1 and stochasticity predictions from Section 5.2. The first finding to consider is that an initial atmosphere mass of 10^{-6} $M_\oplus$ is entirely eroded on all moons with the exception of Titan, and is lost most rapidly on Europa, followed by Ganymede and Callisto. This is in agreement with the time-scales predicted in Section 5.2. From Fig. 8 we can see that the evolution time-scale for an atmosphere with this mass is greater than the entire time span considered in the simulations for Titan, but not for the other four moons. Furthermore, this time-scale is longest for Titan, followed by Callisto, Ganymede, and finally Europa (which is predicted to undergo rapid runaway depletion) in agreement with the results for the initially most massive atmosphere shown in Fig. 9.

Considering next the median atmosphere to planet mass ratios (±1 standard deviation) observed in the numerical results, using Titan as an example, we find that this is $\delta = 10^{(-9.8 \pm 1.1)}$, and order of magnitude lower compared to the analytic prediction of $10^{-8.9}$ made in Section 5.1. The mean atmosphere to planet mass ratio is $\delta = 10^{-8.5}$, slightly higher than this analytic prediction. The analytic prediction, as shown by the vertical line in the right-hand panel of Fig. 9, lies inside the distribution produced by the numerical code, between the median and mean values. As was discussed in Section 5.2, the time-scale over which the atmosphere evolves plays an important role in determining both the stalling mass predicted for the atmosphere and the degree of stochastic variation expected. As the atmosphere is expected to evolve due to small impacts faster than the largest impactors are sampled (assuming the constant impact rate we have adopted) we predicted a decrease in the predicted atmosphere stalling mass compared to the original analytic prediction as well as a degree of stochastic variation for all four outer moons. For Titan specifically, we predicted that the atmosphere would tend towards the stalling mass ratio predicted for a largest impactor size of 10–20 km, approximately $\delta = 10^{-10}$.

We also predicted stochastic variation due to the random accretion of larger objects. This is indeed what we see in the numerical results, with the median atmosphere mass ratio seen for Titan well reproduced by this predicted stalling mass. The upper limit to the absolute atmosphere mass distributions seen for all moons, with the exception of Europa, is approximately 10^{-9} $M_\oplus$, although the value for Callisto is slightly lower and the value for Titan slightly higher. In Section 5.2, we predicted that this limit would be set by the mass of volatiles that could be delivered to the atmosphere mass by a single impact, and for Titan we calculated this to be approximately a few 10^{-9} $M_\oplus$. The value of this upper limit is slightly lower for the other moons due to lower impactor accretion efficiency on these bodies in comparison to Titan.

The same agreement between the numerical results and the stalling masses predicted by the analytic arguments are recreated for the other three moons, with complete atmosphere depletion both predicted and observed in the simulations of Europa. Ganymede and Callisto show similar results, with median atmosphere to planet mass ratios (±1 standard deviation) of $\delta = 10^{(-17 \pm 2)}$ for both. The mean atmosphere mass ratios for these moons are $\delta = 10^{-9.6}$ for Ganymede and $\delta = 10^{-10.3}$ for Callisto. These two values lie either side of the atmosphere stalling mass ratios of $\delta = 10^{-11.5}$ predicted by the analytic method in Section 5.1. In Section 5.2, the time-scale for evolution of Ganymede's argument was used to argue for a lower predicted stalling mass ratio (set by the accretion of 2–5 km objects) of $\delta \sim 10^{-16}$, which is in agreement with the observed numerical results.

These comparisons support the use of the analytic stalling mass prediction, however it is clear there is a large degree of stochastic variation in the atmosphere mass over time which is not captured

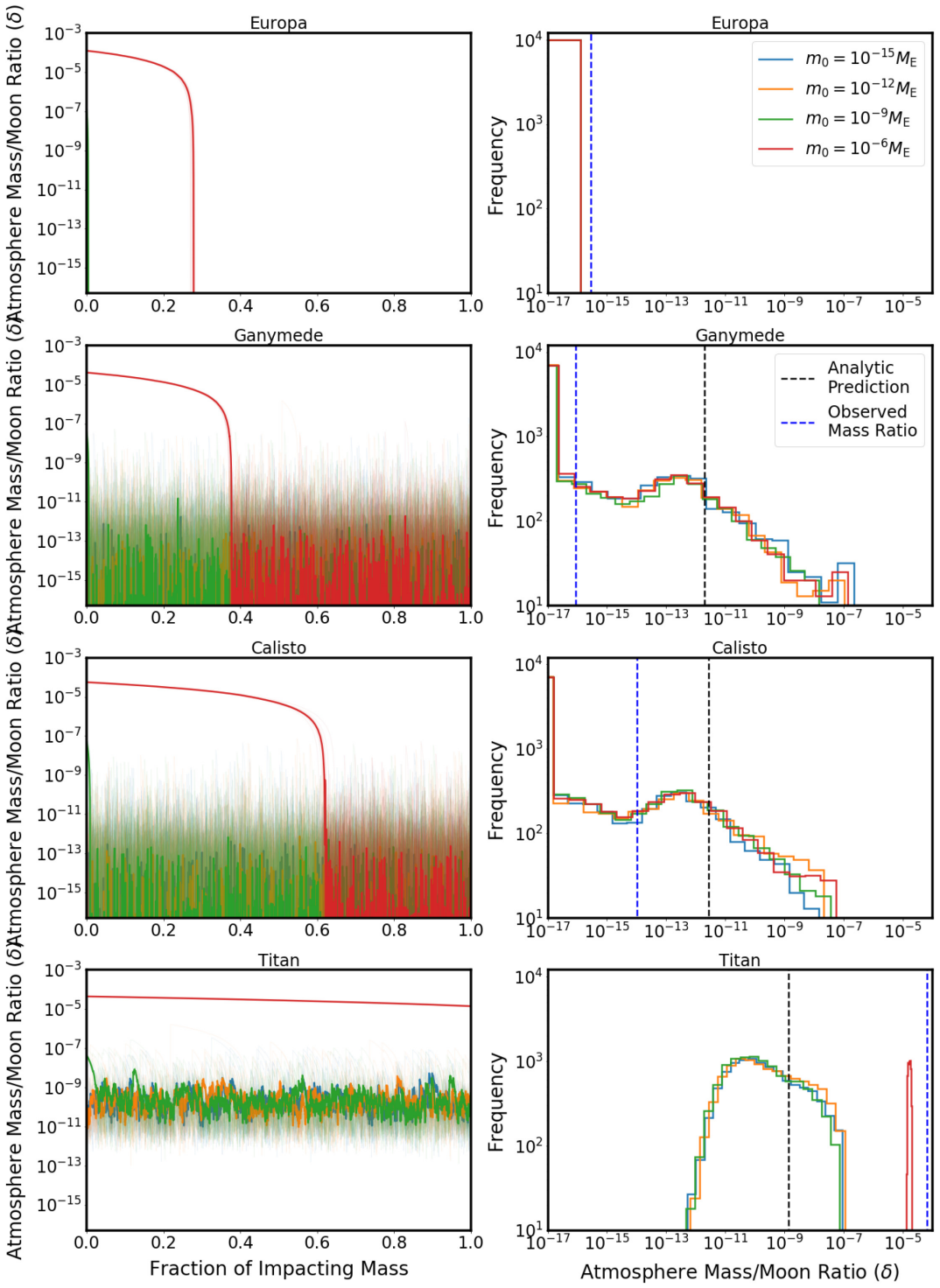

Figure 9. The results of numerical simulations of atmosphere evolution on the four outer moons. The left-hand column illustrates the atmosphere mass through time for a range of initial atmosphere masses shown by different line colours (with M_E in the caption label representing an Earth Mass, $M_\oplus$). Thin thin lines show the ten individual results, and the thick line shows the median mass. The right-hand column shows a histogram of atmosphere masses sampled in the final Gyr over all ten simulations. The lower atmosphere limit (10^{-19} $M_\oplus$) implemented in the code results in an artificial spike in the distribution of observed atmosphere to moon mass ratios, which can be seen in the histograms for Ganymede and Callisto and is the only atmosphere mass recorded for Europa after the initial depletion. The analytic prediction discussed in the text is shown in the right-hand panels by a vertical dashed black line and the observed atmosphere to moon mass ratio is shown by a vertical dashed blue line.

by the analytic prediction. The median atmosphere mass recorded in the numerical results is determined by the accretion of small 1–20 km sized objects that arrive frequently, and determine the quiescent atmosphere level. The mean atmosphere mass is heavily influenced by the stochastic arrival of larger objects that perturb the atmosphere mass to higher values, after which it returns to the quiescent level on a time-scale determined by the assumed impact flux. While we can estimate the size of the largest impactor that will almost certainly impact the moon at some point we cannot say for certain that nothing larger than that object has definitely not arrived. The stochastic nature of our results means that a large degree of variation between the different moons is dependent on the time since the last big impact occurred. Therefore it is possible that the random arrival (or non-arrival) of a particularly significant impact has left an observable imprint on the atmosphere masses and compositions of the outer satellites today. The true nature of impacts on to the outer moons is unlikely to be perfectly represented by the nominal population we consider here, and so in Section 7 we quantify the effect on the atmosphere stalling mass prediction of variation in the impactor composition, size distribution, and velocity distribution. This allows us to understand how robust our predicted results are to this kind of potential variation.

7 SENSITIVITY OF THE ANALYTICALLY PREDICTED STALLING MASS TO THE ASSUMED IMPACTOR PROPERTIES

We can now use the analytic prediction from Section 5 with the knowledge that it is capable of recreating the long-term trends in atmosphere mass (with the caveats on time-scales discussed in Section 5.2) to investigate the sensitivity of the stalling mass predictions to the assumed properties of the impactor population. As in the previous section, these results assume no contribution to the atmosphere from impact-triggered outgassing. As shown in Section 5.2, the size of the largest impactor assumed in the calculation plays a significant role in determining the atmosphere stalling mass and so in the following, unless otherwise specified, the nominal impactor population described in Section 4 with fixed maximum impactor size is used in each case.

7.1 Dependence on impactor density

The previous nominal results have been shown for a variety of impactor densities, but the dependence of the predicted atmosphere stalling mass on this parameter has not yet been discussed. Typically, an increase in the assumed impactor density results in a higher predicted stalling mass. This increase is sharpest at whichever density corresponds to the lowest predicted stalling mass, and in some cases there exists a critical density below which runaway atmospheric depletion is predicted. This critical density is highest for Europa, where impactors would need to have extremely high densities (for a comet) for any amount of atmospheric growth from its current bare state to occur. The other three moons do have stable predicted stalling masses for reasonable assumed comet densities. For densities between 0.75 and 1.25 g cm^{-3} the predicted stalling mass can vary by a few orders of magnitude, and so this is not a negligible effect given the uncertainty in this value. Slight variations in the density of impactors on to the different moons as a result of the stochastic nature of impacts could contribute to the variation in their observed atmosphere masses, but is not sufficient to change their atmosphere masses to the extent seen between Titan and the other moons.

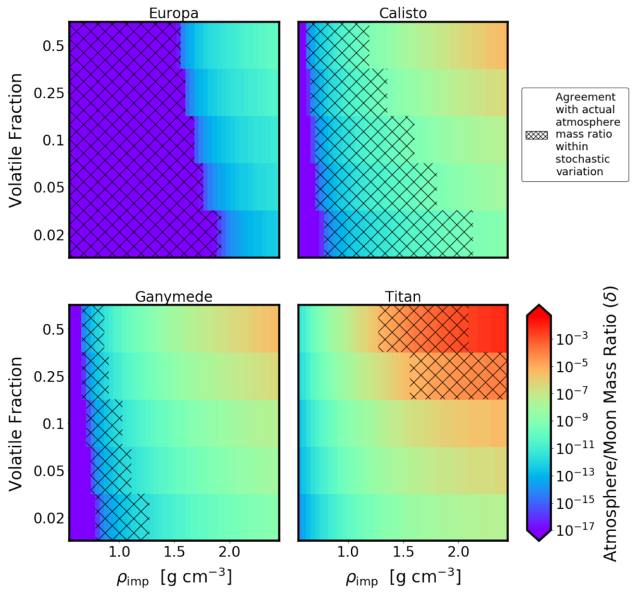

Figure 10. The stalling mass (atmosphere mass at which $f_v = 1$) calculated for the nominal impactor population, as a function of impactor density and impactor volatile fraction for each of the four outer moons. Note that the y axis scale is not linear, and shows results for five values of x_v only. The diagonal hatching shows the region of parameter space in which the predicted stalling mass, plus or minus an amount representative of the stochastic variation observed in the numerical results (calculated as described in the text) for each moon, is in agreement with the estimated atmosphere masses from Table 1.

7.2 Dependence on impactor composition

The nominal results considered only one possible value for the impactor volatile fraction ($x_v = 10$ per cent), and so we investigate the effect of both higher and lower assumed volatile contents here. The atmosphere mass delivered by an impactor population is linearly dependent on the volatile fraction of the impactors (x_v), and thus f_v and the predicted stalling mass are affected by variation in this parameter. Increasing the volatile content of the impactor population will have no noticeable effect on the shape of $f_v(m_{atm})$ shown for the nominal case in Fig. 5, however will shift the entire curve upwards as a result of the increased volatile delivery to the atmosphere.

The predicted atmosphere stalling masses for a range of potential impactor volatile fractions and impactor densities are shown in Fig. 10. As might be expected, increasing the volatile fraction of the impactors increases the value of the stalling mass predicted for a given impactor density. However this effect is much weaker than the dependence on the impactor density. When a stalling mass exists for a given population, this is because f_v decreases with increasing atmosphere mass and crosses one at the stalling mass. Shifting the entire f_v curve upwards will therefore increase the value of the atmosphere mass at which the curve crosses one, leading to a higher predicted stalling mass.

No single impactor density and volatile fraction predicts atmosphere stalling masses that simultaneously match the observed atmosphere mass estimates from Table 1. However we can consider the range of atmosphere masses that might be expected for a single impactor population as a result of the inherently stochastic behaviour of the atmosphere. Based on the numerical results shown in Fig. 9 we calculate the range of $\log_{10}(m_{atm})$ covering 75 per cent of the recorded atmosphere masses for each moon (i.e. the 12.5-th and 87.5-th percentiles of the distributions). This is used to indicate in Fig. 10

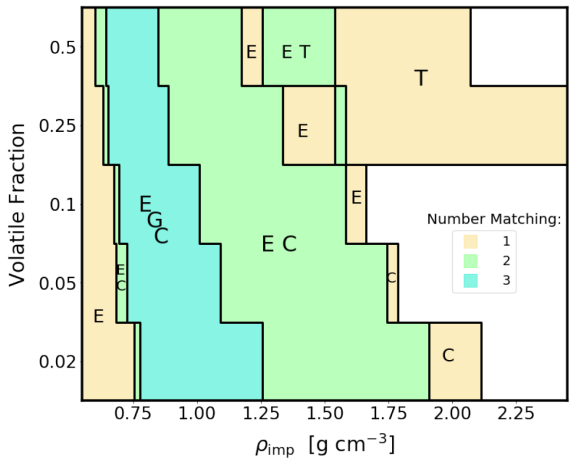

Figure 11. An illustration of number of moons for which the predicted atmosphere stalling mass is in agreement with the estimated atmosphere masses, within representative stochastic variation, as a function of impactor density and impactor volatile fraction, calculated from the results of Fig. 10. The specific moons for which the atmosphere mass is matched are indicated by text annotations on the plot as E (Europa), C (Callisto), G (Ganymede), and T (Titan). The solid black lines show the boundaries in parameter space of this agreement, and the colour of the filled are illustrates the number of moons for which the atmosphere mass is matched. The region of parameter space in which three of these regions overlap, for all the moons except Titan, can be seen to include the nominal impactor composition for cometary impactors.

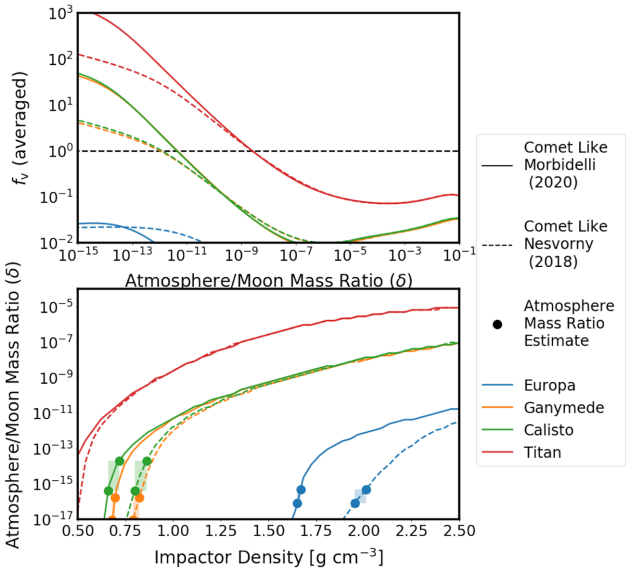

Figure 12. The top panel illustrates a comparison of the behaviour of f_v as a function of atmosphere mass varying the size distribution of the impacting population. The corresponding stalling mass estimates calculated are shown in the bottom panel as a function of impactor density. Each outer satellite is shown by a line of a different colour, while the line style illustrates the size distribution. The region of parameter space in which the predicted stalling mass matches the estimated atmosphere masses for each outer moon from Table 1 are shown by a rectangular shaded area and circular markers.

the range of parameter space in which the predicted atmosphere stalling mass (plus and minus these upper and lower intervals) are in agreement with the observed atmosphere mass estimates.

While no impactor population simultaneously matches all four outer moons, there is a region of parameter space that agrees within these 75 per cent intervals for all four moons with the exception of Titan. In Fig. 11, the boundaries of the hatched regions of parameter space for all four moons are shown, and the number of moons for which there is agreement between the predicted atmosphere stalling mass and the observed atmosphere mass estimates within the stochastic limits is shown as a function of impactor density and volatile fraction. The green region in which there is agreement between the greatest number of moons (all except Titan) includes impactors with the nominal density of 1 g cm^{-3} and nominal volatile content of 10 per cent. Given that we expect the impactor population to have the same composition for all outer moons this agreement indicates a composition within this constrained range, with stochastic variation in the current atmosphere mass introduced by differences among the moons since the most recent large impact. None of the impactor compositions in this region of parameter space are capable of recreating the observed atmosphere mass on Titan, which requires a significant increase in the assumed impactor density for even the most volatile-rich impactors, however as discussed in Section 8 we do not necessarily expect to do this without including impact-triggered outgassing.

7.3 Dependence on impactor size distribution

The size distribution for our nominal impactor population assumes a piece-wise power-law distribution based on that of the objects in the trans-Neptunian disc (Morbidelli et al. 2021). We can consider variation in the differential power-law index, α in comparison to this, adopting an alternative previously published size distribution from Nesvorný et al. (2018). For this, we repeat the calculation of f_v and stalling masses for the full range of impactor densities for each of the four outer satellites. All other parameters are kept the same as the nominal impactor population from Section 4.

The calculated predictions for f_v as a function of atmosphere masses are shown in the top panel of Fig. 12. From this plot, it can be seen that the two size distributions produce similar results at higher atmospheres masses, above approximately $\delta = 10^{-11}$. However at smaller atmosphere masses the Nesvorný et al. (2018) distribution, which contains relatively more of the smallest <km-sized impactors, results in lower values of f_v for a given atmosphere mass (meaning that the tendency for impacts to grow the atmosphere is reduced). The impactor size below which comet-like impactors begin to in general contribute mass to the atmosphere rather than erode mass decreases as the atmosphere mass decreases. For a small atmosphere mass, even km-sized impactors are generally erosive, and thus their relatively larger numbers in the Nesvorný et al. (2018) size distribution result in lower values of f_v.

The corresponding predicted stalling masses are illustrated in the bottom panel of Fig. 12 as a function of impactor density. From this is can be seen that despite the relatively large change in f_v at small atmosphere masses, there is very little difference in the predicted stalling mass for a given impactor density between the two size distributions. This implies that our results are robust to small changes in the slope of the size distribution assumed for the impactors, particularly in comparison to the dependence of the predicted atmosphere mass on the size of the largest impactor.

7.4 Dependence on impactor velocity distribution

Calculation of the stalling mass for a realistic impactor population requires averaging the values of f_v over a distribution of impactor velocities. In the nominal case we have adopted a velocity distribution based on impacts from objects in the Kuiper belt (with $a = 50$ au)

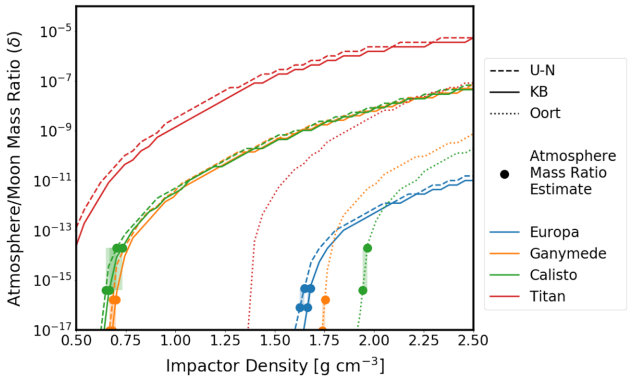

Figure 13. The stalling mass calculated for each of the four outer satellites as a function of impactor density. The different source regions for the impactor populations (and thus the velocity distributions) used to calculate the weighted average of f_v are illustrated by different line styles.

following the method of Zahnle et al. (1992), however this is not the only potential source region for impacts on to the outer satellites.

We can consider three different populations of impactors on to the outer satellites: the Uranus–Neptune planetesimals, Kuiper Belt objects, and Oort cloud objects as discussed in Section 4.2. The stalling masses predicted in the same manner as previously done for the impactor composition and size distribution are shown as a function of impactor density in Fig. 13. As a result of their typically higher impact velocities, the Oort cloud impactors always result in substantially lower stalling masses for a given impactor density and outer satellite compared to the Kuiper Belt objects and Uranus–Neptune planetesimals (which are similar). These predictions are shown by dotted lines in Fig. 13, and are visible only in the lower right-hand corner.

From this figure we can conclude that the predicted stalling masses are relatively insensitive to the assumed velocity distribution of the impactors. However if the impacts were substantially faster than predicted for the Kuiper belt or Uranus–Neptune planetesimal impactor source regions then the stalling mass predictions could be lowered by several orders of magnitude. Slower impactors typically result in greater atmosphere growth, since impactor accretion is higher and atmospheric erosion is lower. Thus a substantially slower distribution of impact velocities could increase the predicted stalling masses. The effect of a potentially slower distribution, that of planetocentric rather than heliocentric impactors, is discussed in Section 9.

8 THE POTENTIAL CONTRIBUTION TO TITAN'S ATMOSPHERE FROM IMPACT-TRIGGERED OUTGASSING

While our results thus do predict greater atmosphere growth and less erosion on Titan in comparison to the Jovian moons, we significantly underpredict the absolute observed atmosphere mass on Titan. There must therefore be an additional source of volatiles. Titan is not only unique among the moons in the outer Solar system for having a massive atmosphere, but also potentially for the volatile-rich composition of its outer layers (Zahnle 2010). As discussed in Section 2.3, a reservoir of trapped volatile species (e.g. in clathrates) in the surface of a body can be released by impact-triggered outgassing. This effect is considered separately from our nominal results due to the large uncertainties in many of the relevant parameters and the simplicity of our toy model. We neglect any

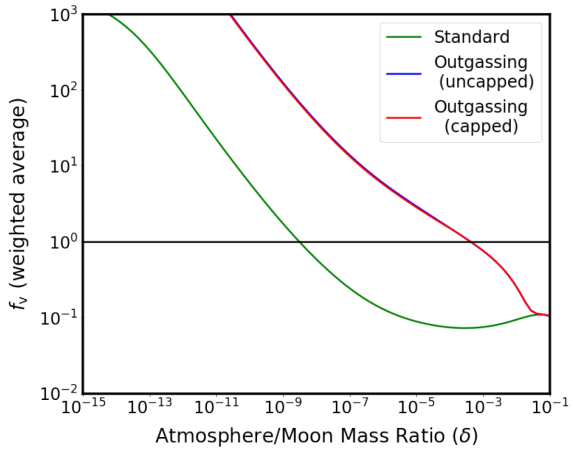

Figure 14. The ratio of atmosphere mass gain to mass-loss as a function of atmosphere mass relative to moon mass for Titan. The solid green line shows the previous calculation of f_v, which did not include any impact-triggered outgassing. The dotted blue line illustrates the values calculated including impact-triggered outgassing, and the dashed red line shows the same including both the volatile content crust limit and the single impact outgassing limit. The predicted atmosphere stalling masses (where $f_v = 1$) calculated for each line are also shown.

chemistry occurring in the atmosphere or as a result of impact shock heating and so the following results are preliminary and do not necessarily capture all of the relevant processes, and so should be interpreted only as evidence that impact-triggered outgassing has the potential to contribute significant volatiles to Titan's atmosphere. In the following, we consider Titan only, as the assumptions made regarding the volatile content of the moons available for outgassing is likely appropriate only for this moon.

8.1 The analytically predicted stalling mass including impact-triggered outgassing

Using our toy model for the mass of outgassed volatiles contributing to the atmosphere mass from Section 2.3, we can calculate again the ratio of atmosphere mass gain to mass-loss, $f_v = \frac{m^+ + m^+_{\rm outgas}}{m^-}$. This can be compared to the previous value, $f_v = \frac{m^+}{m^-}$, to understand how important an effect impact-triggered outgassing is. These computed curves are shown in Fig. 14, as a function of the ratio of atmosphere mass to moon mass. Using this plot, we can compare the behaviour of f_v with atmosphere mass when neglecting impact-triggered outgassing with the behaviour including impact-triggered outgassing with no overall limit on the total mass of outgassed volatiles. This value is not necessarily physical, as it can predict more volatiles released than are estimated to be present in the crust. Therefore we also plot a third version which caps the total contribution to $m^+_{\rm out}$ (the outgassed volatile mass) at the estimated volatile content of the crust.

From this plot, it can be seen that at very high atmosphere masses, impact-triggered outgassing has no effect on the behaviour of the atmosphere, because all impactors are slowed sufficiently whilst passing through the atmosphere to cause no volatile release on impact. However at lower atmosphere masses the additional volatile contribution due to impact-triggered outgassing results in a higher value of f_v for a given atmosphere mass. This results in a larger atmosphere mass at which $f_v = 1$ and thus a larger predicted atmosphere stalling mass.

The predicted stalling masses for these three cases are shown as solid markers in Fig. 14 and can be seen to be highest for the uncapped outgassing prediction and lowest when no impact-triggered outgassing is included. The difference between capped and uncapped predictions is very small and so it is plausible that not all volatiles in the crust have been outgassed. This means that the approach of estimating f_v analytically (which implicitly assumes that all mass delivery and loss mechanisms act over the same time-scale) is overly simplistic. In reality the available volatiles in the crust may be outgassed by the earliest impacts, leading to a large initial atmosphere mass that would then be expected to evolve under the effects of impacts directly on the atmosphere only (i.e. the initial calculation of f_v). We found in Section 6.1 that an initially massive atmosphere is incapable of being eroded by impacts even when neglecting the contribution from outgassing.

8.2 Implications of outgassing on the methane in Titan's atmosphere

The methane component of Titan's atmosphere is estimated to have a total mass of 2.8×10^{20} g $\approx 5 \times 10^{-8}$ $M_\oplus$ ($\delta \sim 2 \times 10^{-6}$) (Lunine & Stevenson 1987; Choukroun et al. 2010) and should rapidly undergo photolysis and be irreversibly lost from the atmosphere on a time-scale of 10–100 Myr (Yung, Allen & Pinto 1984; Toublanc et al. 1995; Lunine & Atreya 2008). There must therefore be a continuing source of methane (Owen 2004). Exogenous delivery by cometary impacts is unlikely due to the low current impact rate and the lack of CO (which should be delivered by comets) detected in the atmosphere (Choukroun et al. 2010). Episodic outgassing from clathrate hydrates in the crust has been proposed as a potential explanation for this phenomenon (Tobie et al. 2006; Stofan et al. 2007). Below we discuss two ways that impact-triggered outgassing could contribute the $\sim 5 \times 10^{-8}$ $M_\oplus$ budget of CH_4 to Titan's atmosphere within the last 10–100 Myr.

First, a single stochastic impact could cause the catastrophic outgassing of this mass of CH_4 in a single event. Based on our prescription for impact-triggered outgassing, a single impact on to Titan could release this mass of methane (assuming a surface volatile fraction of $x_{v,targ} = 1$ per cent and that the outgassed material is 50 per cent CH_4) if it had a mass of $\sim 3 \times 10^{-7}$ $M_\oplus$, corresponding to a comet-like impactor size of 158 km. This impactor size is larger than the largest size expected to be sampled at the current impact rate as discussed in Section 5.3, however as previously discussed, the stochastic sampling of larger objects is to be expected, and so while it is unlikely, it is not entirely implausible that a relatively recent large impact triggered the outgassing of the current budget of methane in Titan's atmosphere.

Alternatively, we can ask whether the continued accretion of small objects over the last 10–100 Myr is capable of cumulatively outgassing the observed methane. The current impact rate on to Titan is approximately 1.4×10^{-11} $M_\oplus$ Myr^{-1}, which over 10–100 Myr results in the accretion of an approximate impactor mass of $(1.4 - 14) \times 10^{-10}$ $M_\oplus$, corresponding to objects up to roughly 10 km in size as discussed in Section 5.3. Assuming the nominal velocity distribution and accounting for atmospheric drag assuming the current atmosphere mass on Titan, equations (12) to (14) tell us that these objects have an outgassing efficiency of ~0.01, meaning that at most $\sim 10^{-9}$ $M_\oplus$ of CH_4 is able to be outgassed over this time period. This is lower than the estimated methane budget in Titan's atmosphere, and so continued outgassing from Titan's surface as a result of the current level of bombardment is unlikely to fully replenish the atmospheric methane.

9 DISCUSSION

We have found that our nominal predicted stalling masses recreate the depletion of Europa's atmosphere for a reasonable estimated impactor density, and estimate stalling masses that are consistent with the observed low atmosphere masses on Callisto and Ganymede. By including impact-triggered outgassing on Titan we are then able to match the observation of a thick atmosphere on this moon. We have also found that stochastic effects, both over time for the same moon and between the moons is a significant source of variation in the predicted atmosphere masses. While our results suggest that the inevitable impacts that occur on these moons have shaped their atmospheric evolution we have neglected several other processes that can alter the atmosphere: thermal (Jeans) escape, XUV driven escape, magnetospheric effects (atmosphere drag as well as ion delivery), and continuing outgassing from the solid material of the moon. The magnitude of these effects will vary between the moons, due to their different masses, environments (in the Solar system and relative to their host) and atmospheres. As a result of this, effects that may be negligible on one moon may be significant on others.

9.1 Titan

The potential existence of a population of planetocentric (rather than heliocentric) impactors was used in Farinella, Marzari & Matteoli (1997) to propose an origin for Titan's thick atmosphere, using material accreted after the disruption of a hypothetical 'proto-Hyperion'. These impacts were assumed to be significantly slower (<4 km s^{-1}) and thus material was accreted efficiently, growing a thick atmosphere. However, there are other explanations proposed for the origin and evolution of Titan's atmosphere, a topic which has long been debated (Niemann et al. 2010). The atmospheric D-H ratio, as well as the excess CH_4 compared to CO, both disfavour cometary material as the direct source of Titan's atmosphere (Coustenis 2005), but do not exclude the possibility that impacts could trigger outgassing of volatiles contained within Titan.

The most probable source of atmospheric N_2 is either ammonia (NH_3) which can later be decomposed through either photolysis (Atreya, Donahue & Kuhn 1978) and impact-mediated chemistry (Sekine et al. 2011), or N_2 directly outgassed through thermal decomposition of chondritic insoluble organic material in the interior (Miller, Glein & Waite 2019). The enrichment of ^{15}N relative to ^{14}N in the atmosphere compared to the terrestrial atmosphere value cannot be achieved by conversion of NH_3 to N_2 alone. If the original source of nitrogen in both Titan and Earth is the same, then this discrepancy (as well as other heavy isotope anomalies) might imply significant loss of N_2 from Titan's atmosphere early in its history, when the Solar XUV flux was higher (Coustenis 2005; Penz et al. 2005; Waite et al. 2005; Lammer et al. 2008). This is not necessarily in disagreement with our conclusions. As discussed in Section 8, the mass of volatiles that can be outgassed into the atmosphere is sensitive to the upper limit assumed for volatiles in the crust. A higher value for this limit could result in a much more massive early atmosphere that could then be lost through hydrodynamic escape as suggested in Lammer et al. (2008).

9.2 Ganymede

We have neglected magnetic effects in our model, which are likely to be important in particular on Ganymede, the only moon that possesses a permanent intrinsic magnetic dipole, as well as an induced dipole arising from Jupiter's magnetosphere (Kivelson et al.

2002). While this field is dominated by Jupiter's own magnetic field it is believed to be the source of the asymmetric molecular oxygen air glow (caused by electron dissociation of O_2 on the surface) that was observed by *HST* (Hall et al. 1998). Magnetospheric effects have been proposed as both a source of atmosphere material and as a loss mechanism. The magnetosphere on Ganymede is too weak to protect the surface from energetic particles in the Jovian magnetic field, resulting in release of oxygen ions from the surface by plasma sputtering (Carnielli et al. 2020). Ion pickup can accelerate atmospheric material to above the escape velocity, resulting in atmospheric loss also (Luhmann & Kozyra 1991; Lundin, Lammer & Ribas 2007). The intrinsic and extrinsic magnetic fields undergo complex interactions, and the interactions between them and the atmosphere is not trivial, meaning it is challenging to predict what effect their inclusion may have on our atmosphere stalling mass predictions. However our prediction for the atmosphere mass is likely relevant for the early atmosphere of Ganymede, when impact rates were high and the effect of impacts would be expected to dominate. Since that time, impacts continue to erode the atmosphere and deliver material at a rate that depends on the atmosphere mass, which is a contribution that should be factored into a model that considers the evolution of the atmosphere due to magnetospheric effects.

9.3 Callisto

The tenuous CO_2 component of Callisto's current atmosphere was previously believed to be so tenuous that it should be lost almost immediately as a result of photoionization and magnetic effects and so must be being constantly replenished, potentially by sublimation of CO_2 ice from the surface (Carlson 1999). However the much more massive O_2 component inferred from the ionosphere is not expected to be lost on such a short time-scale. These effects are not easily parametrized and so not included in our model, but an extra sink term acting to remove atmosphere mass could shift the predicted atmosphere mass from our predicted value downwards. Since CO_2 is an expected product when the CO present in comets is shocked in the presence of H_2O during an impact (Ishimaru et al. 2011), the potential role of comet impacts in supplying CO_2 ice to Callisto's surface is worth future study. We find that impact by the nominal comet population can deliver a mass of $10^{17} - 10^{18}$ kg in solid material to the surface of Callisto (and a similar mass to the other moons) which is likely to contain a substantial mass of CO and CO_2, alongside water ice and other material. Spectra of the surface of Callisto show similar signatures to interstellar ice grains, hinting at the possibility that these grains have been delivered by cometary material (Johnson 2014).

9.4 Europa

The origin of Europa's atmosphere is believed to be radiative dissociation of water molecules on the surface into oxygen and hydrogen, which are then adsorbed and sputtered into the atmosphere. The hydrogen escapes rapidly, and any water is rapidly frozen back on to the surface, leaving oxygen to make up the bulk of the tenuous atmosphere (Ip et al. 1998; Lucchetti et al. 2016; Li, Gudipati & Yung 2020). Escaped gas molecules form a torus of H_2 and O distributed around Europa's orbit which has been detected by Cassini and Galileo (Smyth & Marconi 2006). We have demonstrated that impacts are not capable of growing a substantial atmosphere on Europa, however the potential for comets to deliver some portion of the water that subsequently dissociated to form the surface of the moon has not been explored. The estimated non-volatile mass delivered by comets in our model ($10^{17} - 10^{18}$ kg) will contain water ice, which may contribute to this atmosphere source reservoir.

10 CONCLUSION

In conclusion, we have investigated the effect that impacts can have on the atmospheres of four satellites of the giant planets, Ganymede, Callisto, Europa, and Titan. Using the numerical code developed in Sinclair et al. (2020) we model the evolution of these atmospheres under bombardment by a nominal population of impactors assumed to be similar to ecliptic comets originating in the Kuiper Belt. For this nominal population we have constructed distributions of size and velocity from which impactors are sampled and their effect on the atmosphere calculated.

The numerical code was used to predict the atmospheric evolution for a range of initial atmosphere masses. From our results we find that the predicted atmosphere masses vary by many orders of magnitude both between iterations of the code and within single iterations due to the inherently stochastic nature of impacts on to the outer moons, which is an important effect to consider.

We also develop an analytic approximation for the 'stalling mass', based on the behaviour of the parameter f_v (the ratio of atmosphere mass gain to mass loss) as a function of atmosphere mass. This equilibrium atmosphere mass, while not predicted by some previous studies, arises when the same impacting population is capable of both eroding a massive atmosphere and delivering volatiles to a bare target. This occurs in the energy scaling Shuvalov (2009) impact prescription, but not the inertia scaling model from Melosh & Vickery (1989). We have shown that over sufficiently long timescales, the median atmosphere mass from the numerical code is successfully predicted by the analytic argument. This analytic stalling mass for the nominal population of impactors predicts complete erosion of Europa's atmosphere and depletion to very low levels on Ganymede and Callisto. While the current rarefied atmospheres of these bodies are not impact-generated, our results suggest that impacts would not be capable of growing a large atmosphere that would subsequently need to be lost through another mechanism. The analytic stalling mass predicted for Titan is orders of magnitude more massive than the other moons, but still is significantly lower than the observed atmosphere mass.

The sensitivity of our predicted stalling masses to the properties of the impactor population was considered. We find that the volatile content is a less important parameter than the bulk impactor density, but is still capable of increasing the predicted stalling mass by a factor of approximately 100 over a range of $x_v = 2 - 50$ per cent. The impactor density can have a significantly larger effect on the stalling mass, increasing it by several orders of magnitude between $\rho_{imp} = 0.5 - 2.0$ g cm^{-3}. The slope of the size distribution has a relatively small effect on the predicted stalling mass, however the size of the largest impactor used in the calculation does play an important role. This size is determined by the time-scale over which impacts are sampled from the parent population and thus over which the atmosphere evolves. On longer time-scales, the largest sampled impactor size increases and this acts to increase the predicted atmosphere stalling mass. This dependence is stronger on short time-scales as the nominal comet-like size distribution contains relatively few of the larger impactors. Finally, the dependence of the stalling mass on the assumed velocity distribution of the impactors is small when the impactors are assumed to originate in the region just exterior to Neptune, but is significantly reduced when the source region is the Oort cloud, since this results in significantly faster impactors that are

far more erosive to the atmosphere. The potential for significantly slower planetocentric impactors resulting from disrupted objects captured by the host planet would result in decreased atmospheric erosion and more impactor accretion, increasing the stalling mass.

When including a simple model for the effect of impact-triggered outgassing we find that this additional source of volatiles is capable of providing the mass needed to match Titan's current atmosphere. This level of outgassing requires the existence of a volatile-rich crust (something that is potentially not applicable to the Jovian moons) and so these results are applicable only to Titan. The predicted atmosphere stalling masses when including impact-triggered outgassing are sensitive to the assumed volatile content of the crust and the outgassing efficiency, both of which are not well constrained.

Our results suggest that impacts have played a significant role in shaping the atmospheres on the outer moons. While there are doubtless many other processes acting to deliver and remove volatiles from the atmospheres on these moons, our results suggest it is challenging to sustain any significant atmosphere on the moons of Jupiter during a period of bombardment, whilst impacts are less damaging to atmospheres on Titan. We also find that the effects of stochasticity are significant and capable of introducing orders of magnitude variation in the atmosphere mass that must be accounted for when considering the evolution of these atmospheres. More detailed observations of the atmospheres of the Jovian moons by JUICE and Titan's atmospheric composition by Dragonfly will help us to constrain the potential sources and evolutionary processes of the atmospheres on these outer moons (Wurz et al. 2014).

ACKNOWLEDGEMENTS

CAS acknowledges the support of STFC via the award of a DTP Ph.D. studentship.

DATA AVAILABILITY

Data available on request.

REFERENCES

Alibert Y., Mousis O., 2007, A&A, 465, 1051
Anderson J. D., Jacobson R. A., McElrath T. P., Moore W. B., Schubert G., Thomas P. C., 2001, Icarus, 153, 157
Artemieva N., Lunine J. I., 2005, Icarus, 175, 522
Atreya S. K., Donahue T. M., Kuhn W. R., 1978, Science, 201, 611
Bell S. W., 2020, J. Geophys. Res., 125, e06392
Broadfoot A. L. et al., 1981, J. Geophys. Res., 86, 8259
Carlson R. W., 1999, Science, 283, 820
Carnielli G., Galand M., Leblanc F., Modolo R., Beth A., Jia X., 2020, Icarus, 351, 113918
Cataldi G., Brandeker A., Thébault P., Singer K., Ahmed E., de Vries B. L., Neubeck A., Olofsson G., 2017, Astrobiology, 17, 721
Catling D. C., Kasting J. F., 2017, Atmospheric Evolution on Inhabited and Lifeless Worlds. Cambridge Univ. Press, Cambridge
Choukroun M., Grasset O., Tobie G., Sotin C., 2010, Icarus, 205, 581
Coustenis A., 2005, Space Sci. Rev., 116, 171
Cunningham N. J., Spencer J. R., Feldman P. D., Strobel D. F., France K., Osterman S. N., 2015, Icarus, 254, 178
Denman T. R., Leinhardt Z. M., Carter P. J., Mordasini C., 2020, MNRAS, 496, 1166
Farinella P., Marzari F., Matteoli S., 1997, AJ, 113, 2312
Feldman P. D., McGrath M. A., Strobel D. F., Moos H. W., Retherford K. D., Wolven B. C., 2000, ApJ, 535, 1085
Festou M. C., Keller H. U., Weaver H. A., 2004, Comets II. University of Arizona Press, Tucson
Griffith C. A., Zahnle K., 1995, J. Geophys. Res., 100, 16907
Hall D. T., Strobel D. F., Feldman P. D., McGrath M. A., Weaver H. A., 1995, Nature, 373, 677
Hall D. T., Feldman P. D., McGrath M. A., Strobel D. F., 1998, ApJ, 499, 475
Hand K. P., Chyba C. F., Carlson R. W., Cooper J. F., 2006, Astrobiology, 6, 463
Hörst S. M., 2017, J. Geophys. Res., 122, 432
Housen K. R., Holsapple K. A., 2011, Icarus, 211, 856
Iess L. et al., 2012, Science, 337, 457
Ip W. H., Williams D. J., McEntire R. W., Mauk B. H., 1998, Geophys. Res. Lett., 25, 829
Ishimaru R., Sekine Y., Matsui T., Mousis O., 2011, ApJ, 741, L10
Johnson T., 2014, in Holland H. D., Turekian K. K., eds, Treatise on Geochemistry (Second Edition), second edition edn. Elsevier, Oxford, p. 313
Johnson R. E., Leblanc F., Yakshinskiy B. V., Madey T. E., 2002, Icarus, 156, 136
Kegerreis J. A., Eke V. R., Catling D. C., Massey R. J., Teodoro L. F. A., Zahnle K. J., 2020 , ApJ, 901, L31
Kivelson M. G., Khurana K. K., Volwerk M., 2002, Icarus, 157, 507
Korycansky D., Zahnle K., 2005, Planet. Space Sci., 53, 695
Kral Q., Wyatt M. C., Triaud A. H. M. J., Marino S., Thébault P., Shorttle O., 2018, MNRAS, 479, 2649
Kraus R. G., Senft L. E., Stewart S. T., 2011, Icarus, 214, 724
Lammer H., Kasting J. F., Chassefière E., Johnson R. E., Kulikov Y. N., Tian F., 2008, Space Sci. Rev., 139, 399
Leinhardt Z. M., Stewart S. T., 2012, ApJ, 745, 79
Li J., Gudipati M. S., Yung Y. L., 2020, Icarus, 352, 113999
Liang M.-C., Lane B. F., Pappalardo R. T., Allen M., Yung Y. L., 2005, J. Geophys. Res., 110, 1
Lucchetti A., Plainaki C., Cremonese G., Milillo A., Cassidy T., Jia X., Shematovich V., 2016, Planet. Space Sci., 130, 14
Luhmann J. G., Kozyra J. U., 1991, J. Geophys. Res., 96, 5457
Lundin R., Lammer H., Ribas I., 2007, Space Sci. Rev., 129, 245
Lunine J., Atreya S., 2008, Nat. Geosci., 1, 335
Lunine J. I., Stevenson D. J., 1987, Icarus, 70, 61
Mah J., Brasser R., 2019, MNRAS, 486, 836
Marounina N., Tobie G., Carpy S., Monteux J., Charnay B., Grasset O., 2015, Icarus, 257, 324
McKinnon W. B., Kirk R. L., 2014, in Spohn T., Breuer D., Johnson T. V., eds, Encyclopedia of the Solar System (Third Edition), third edition edn. Elsevier, Boston, p. 861
Melosh H. J., Vickery A. M., 1989, Nature, 338, 487
Miller K. E., Glein C. R., Waite J. Hunter J., 2019, ApJ, 871, 59
Morbidelli A., Nesvorny D., Bottke W. F., Marchi S., 2021, Icarus, 356, 114256
Nesvorný D., Vokrouhlický D., Morbidelli A., 2013, AJ, 768, 45
Nesvorný D., Vokrouhlický D., Dones L., Levison H. F., Kaib N., Morbidelli A., 2017, ApJ, 845, 27
Nesvorný D., Vokrouhlický D., Bottke W. F., Levison H. F., 2018, Nat. Astron., 2, 878
Niemann H. B. et al., 2010, J. Geophys. Res., 115, E12006
Owen T. C., 2004, AGU Fall Meeting Abstracts, P42A–01
Penz T., Lammer H., Kulikov Y., Biernat H., 2005, Adv. Space Res., 36, 241
Schlichting H. E., Sari R., Yalinewich A., 2015, Icarus, 247, 81
Sekine Y., Genda H., Sugita S., Kadono T., Matsui T., 2011, Nat. Geosci., 4, 359
Shoemaker E. M., Wolfe R. F., 1982, in Morrison D., ed., Satellites of Jupiter. University of Arizona Press, Tucson, p. 277
Shuvalov V., 2009, Meteor. Planet. Sci., 44, 1095
Shuvalov V., Kührt E., de Niem D., Wünnemann K., 2014, Planet. Space Sci., 98, 120
Sinclair C. A., Wyatt M. C., Morbidelli A., Nesvorný D., 2020, MNRAS, 499, 5334
Smyth W. H., Marconi M. L., 2006, Icarus, 181, 510
Sohl F., Spohn T., Breuer D., Nagel K., 2002, Icarus, 157, 104
Stofan E. R. et al., 2007, Nature, 445, 61
Strobel D. F., 1982, Planet. Space Sci., 30, 839

Strom R. G., Croft S. K., 1993, in Lunar and Planetary Science Conference. Lunar and Planetary Science Conference. p. 1373
Svetsov V. V., 2007, Sol. Syst. Res., 41, 28
Tobie G., Lunine J. I., Sotin C., 2006, Nature, 440, 61
Toublanc D., Parisot J. P., Brillet J., Gautier D., Raulin F., McKay C. P., 1995, Icarus, 113, 2
Waite J. H. et al., 2005, Science, 308, 982
Waite J. H. J. et al., 2009, Nature, 460, 1164
Walker J. C. G., 1986, Icarus, 68, 87
Wurz P. et al., 2014, in European Planetary Science Congress. p. EPSC2014–504
Wyatt M. C., Kral Q., Sinclair C. A., 2020, MNRAS, 491, 782
Yung Y. L., Allen M., Pinto J. P., 1984, ApJS, 55, 465
Zahnle K., 2010, in Cottini V., Nixon C., Lorenz R., eds, Through Time; A Workshop On Titan's Past, Present and Future. p. 25
Zahnle K., Pollack J. B., Grinspoon D., Dones L., 1992, Icarus, 95, 1
Zahnle K., Schenk P., Levison H., Dones L., 2003, Icarus, 163, 263
Zebker H. A., Stiles B., Hensley S., Lorenz R., Kirk R. L., Lunine J., 2009, Science, 324, 921
Zhu M., Artemieva N., Morbidelli A., Yin Q., Becker H., Wünnemann K., 2019, Nature, 571, 2226

APPENDIX A: VELOCITY DISTRIBUTION DERIVATION

Assume that all the comets have a single semimajor axis, uniform pericentre distributions (from $p_{\rm min}$ to $p_{\rm max}$), and isotropic inclination distributions from $i = 0 - i_{\rm max}$. The heliocentric distributions are thus $n(a, p, i)\,{\rm d}a\,{\rm d}p\,{\rm d}i$. The relative velocity (at infinity) between such a comet and a planet with orbital velocity $v_{\rm tar}$ is

$$v_\infty^2 = \xi^2 v_{\rm tar}^2 = v_{\rm tar}^2 \left(3 - \frac{a_{\rm tar}}{a} - 2\cos(i)\sqrt{\frac{p}{a_{\rm tar}}\left(2 - \frac{p}{a}\right)}\right). \quad \text{(A1)}$$

Once the comet is within the region of the planet, we need to know whether or not it will impact the moon. The impact parameter (b) on to a satellite with orbital velocity $v_{\rm sat}$ is given by $bv_\infty = rv_{\rm t}$, where $v_{\rm t}$ is the tangential velocity of the comet at a distance r from the satellite. The maximum impact parameter occurs when $r = a_{\rm sat}$ and $v_t = v = \sqrt{v_\infty^2 + 2v_{\rm sat}^2}$, and is thus

$$b_{\rm max} = r\frac{v_{\rm t}}{v_\infty} = a_{\rm sat}\sqrt{1 + 2\frac{v_{\rm sat}^2}{v_\infty^2}}. \quad \text{(A2)}$$

The impact parameter is then assumed to follow a uniform distribution between 0 and this value of $b_{\rm max}$.

The inclination of the comet relative to the satellite plane (i') is assumed to be isotropic such than $\cos(i')$ is uniformly distributed between 0 and 1. In the coordinate system centred on the planet, the satellite and comet have velocities of $\mathbf{v}_{\rm sat} = (0, v_{\rm sat}, 0)$ and $\mathbf{v}_{\rm com} = (v_{\rm r}, v_{\rm t}\cos(i'), v_{\rm t}\sin(i'))$. The relative velocity is therefore

$$v_{\rm rel}^2 = |\mathbf{v}_{\rm sat} - \mathbf{v}_{\rm com}| = v_\infty^2 + 3v_{\rm sat}^2 - 2v_{\rm t}v_{\rm sat}\cos(i'). \quad \text{(A3)}$$

The impact velocity (including gravitational focusing) is thus

$$v_{\rm imp}^2 = v_{\rm rel}^2 + v_{\rm esc}^2 = v_\infty^2 + 3v_{\rm sat}^2 - 2v_{\rm t}v_{\rm sat}\cos(i') + v_{\rm esc}^2. \quad \text{(A4)}$$

According to Zahnle et al. (1992), following Shoemaker & Wolfe (1982) gives the collision probability for each comet to be proportional to

$$P_{\rm col} \propto \left(1 + 2\frac{v_{\rm sat}^2}{v_\infty^2}\right)\left(1 + \frac{v_{\rm esc}}{v_\infty^2 + 2v_{\rm sat}^2}\right)\frac{\xi}{\xi_x\sin(i')}, \quad \text{(A5)}$$

where the radial component of the dimension-less parameter ξ is

$$\xi_x^2 = 2 - \frac{a_{\rm tar}}{a} - \frac{p}{a_{\rm tar}}\sqrt{2 - \frac{p}{a}}. \quad \text{(A6)}$$

This paper has been typeset from a TEX/LATEX file prepared by the author.